# Transcriptional inhibition after irradiation occurs preferentially at highly expressed genes in a manner dependent on cell cycle progression

Zulong Chen[1,^], Xin Wang[2,3,^], Xinlei Gao[2,3], Nina Arslanovic[1], Kaifu Chen[2,3,*] and Jessica Tyler[1,*]

[1]Weill Cornell Medicine, Department of Pathology and Laboratory Medicine, New York, NY 10065, USA

[2]Basic and Translational Research Division, Department of Cardiology, Boston Children's Hospital, Boston, MA 02115, USA

[3]Department of Pediatrics, Harvard Medical School, Boston, MA 02115, USA

^Equal contribution

[*]Corresponding Authors: jet2021@med.cornell.edu, kaifu.chen@childrens.harvard.edu

**Abstract**

In response to DNA double strand damage, ongoing transcription is inhibited to facilitate accurate DNA repair while transcriptional recovery occurs after DNA repair is complete. However, the mechanisms at play and identity of the transcripts being regulated in this manner are unclear. In contrast to the situation following UV damage, we found that transcriptional recovery after ionizing radiation (IR) occurs in a manner independent of the HIRA histone chaperone. Sequencing of the nascent transcripts identified a programmed transcriptional response, where certain transcripts and pathways are rapidly downregulated after IR, while other transcripts and pathways are upregulated. Specifically, most of the loss of nascent transcripts occurring after IR is due to inhibition of transcriptional initiation of the highly transcribed histone genes and the rDNA. To identify factors responsible for transcriptional inhibition after IR in an unbiased manner, we performed a whole genome gRNA library CRISPR / Cas9 screen. Many of the top hits in our screen were factors required for protein neddylation. However, at short times after inhibition of neddylation, transcriptional inhibition still occurred after IR, even though neddylation was effectively inhibited. Persistent inhibition of neddylation blocked transcriptional inhibition after IR, and it also leads to cell cycle arrest. Indeed, we uncovered that many inhibitors and conditions that lead to cell cycle arrest in $G_1$ or $G_2$ phase also prevent transcriptional inhibition after IR. As such, it appears that transcriptional inhibition after IR occurs preferentially at highly expressed genes in cycling cells.

40 **Introduction**

41 DNA double strand breaks (DSB) are one of most deleterious types of DNA lesions. Failure to
42 repair a single DSB can lead to loss of a chromosome arm or cell death and inaccurate repair can
43 lead to changes such as insertions, deletions, and translocations. Accordingly, the cell has
44 developed an intricate DNA damage response (Jackson and Bartek, 2009). In vertebrate cells, the
45 DNA damage response is mediated through activation of three PI3-like kinases: ataxia
46 telangiectasia mutated (ATM), Ataxia telangiectasia and Rad3-related (ATR) and DNA
47 dependent protein kinase (DNA-PK) (Blackford and Jackson, 2017), which coordinates DNA
48 repair and the DNA damage cell cycle checkpoint which arrests cells until DSBs are repaired.

49

50 Additionally, ATM and DNA-PK have been shown to inhibit transcription in response to DSBs in
51 a manner that occurs so transiently that it can only be detected when examining the nascent, not
52 bulk, transcripts (Pankotai and Soutoglou, 2013). The transcription resumes or "recovers"
53 immediately after DSB repair (Pankotai and Soutoglou, 2013). This transient inhibition of
54 transcription after DSBs was initially shown for RNA polymerase I (Pol I) transcripts, where ATM
55 triggered the reduction of nascent ribosomal gene transcripts, shown by visualization of a labelled
56 ribonucleotide analog within the nucleolus, after exposure to ionizing radiation (IR) (Kruhlak et
57 al., 2007). Mechanistically, the DSBs triggered a reduction in Pol I initiation complex assembly
58 and led to premature displacement of elongating Pol I from the rDNA genes (Kruhlak et al., 2007).
59 Using a reporter that allowed for visualization of repair protein recruitment and local transcription
60 within cells, it was subsequently shown that ATM also mediates the inhibition of RNA polymerase
61 II (Pol II) transcriptional elongation of genes in the vicinity of I-SceI endonuclease induced DSBs
62 (Shanbhag et al., 2010). This transcriptional inhibition was partly dependent on the E3 ubiquitin

63 ligases RNF8 and RNF168, whereas transcriptional recovery depended on the USP16 enzyme that
64 deubiquitylates histone H2A (Shanbhag et al., 2010). Additional mechanistic analyses using this
65 same system revealed that ATM dependent phosphorylation of the ATP-dependent nucleosome
66 remodeler PBAF is required for local transcriptional inhibition of Pol II transcription flanking a
67 DSB (Kakarougkas et al., 2014), indicating that chromatin changes are also required for
68 transcriptional inhibition in response to DSBs. The purpose of local transcriptional inhibition is to
69 allow efficient and accurate DSB repair (Kakarougkas et al., 2014, Meisenberg et al., 2019).
70 Polycomb group proteins and cohesin have also been shown to be required for local transcriptional
71 inhibition of Pol II transcription flanking a DSB, although their role is unclear (Meisenberg et al.,
72 2019, Kakarougkas et al., 2014), further indicating that chromatin structure and potentially
73 chromosome architecture also regulate transcriptional inhibition in response to DSBs.
74
75 Somewhat surprisingly, a distinct mechanism has been reported for the inhibition of Pol II
76 transcription at genes containing a DSB induced by the endonuclease I-PpoI (Pankotai et al., 2012).
77 In this case, both Pol II initiation and elongation were reduced adjacent to the DSB, in a manner
78 dependent on DNA-PK and the proteasome (Pankotai et al., 2012). Mechanistically, DNA-PK
79 appeared to help recruit the E3 ubiquitin ligase WWP2 to DSBs, which then promoted the
80 proteosome-dependent eviction of Pol II (Caron et al., 2019). In the absence of WWP2, the DNA
81 repair machinery was not efficiently recruited, indicating again that the reason for transcriptional
82 inhibition *in cis* flanking a DSB is to promote DNA repair (Caron et al., 2019). The papers
83 examining transcriptional inhibition around DSBs induced by endonucleases generally find the
84 transient repression occurs locally or *in cis* to the DSB (Iannelli et al., 2017). However, another
85 study found induction of the same set of ~ 200 transcripts soon after irradiation and endonuclease

86 break induction that occurred in a manner dependent on ATM and p53, while only 33 nascent
87 transcripts were down regulated after DSB induction (Venkata Narayanan et al., 2017). Yet
88 another study found that more genes were repressed than induced after inducing global DSBs with
89 neocarzinostatin, and this occurred via p53 mediated down-regulation of MYC (Porter et al.,
90 2017). As such, there are contradictory findings in the field at present. Furthermore, the mechanism
91 of transcriptional recovery after DSB repair is far from clear. In response to UV damage, global
92 transcriptional inhibition and recovery occurs, and this transcriptional recovery after UV repair is
93 dependent on the histone variant H3.3 histone chaperone HIRA (Bouvier et al., 2021, Adam et al.,
94 2013). Mechanistically, HIRA functioned to repress the transcriptional repressor ATF3, in turn
95 promoting transcriptional recovery after UV repair (Bouvier et al., 2021).
96
97 In contrast to the studies to date that have only examined local transcription inhibition occurring
98 *in cis* after DSB damage, we sought to examine transient transcriptional inhibition after induction
99 of global DSBs by IR exposure, and the subsequent transcriptional recovery after DSB repair, via
100 fluorescent labelling of a ribonucleotide analog incorporated only into nascent transcripts. Unlike
101 the situation following UV repair, we do not find a role for HIRA in transcriptional recovery after
102 DSB repair. Our sequencing of the nascent transcripts after irradiation identified a programmed
103 transcriptional program where a larger number of protein-coding genes were upregulated than
104 downregulated. The genes that were immediately downregulated after IR tended to be highly
105 transcribed genes including the rRNAs and histones, while the upregulated genes tended to be
106 transcribed at a lower level. We developed a flow cytometry-based assay of nascent transcripts
107 and used it as the basis for a whole genome gRNA screen to identify factors required for
108 transcriptional inhibition after IR. In addition to finding ATM as being required for inhibition of

109 transcription after DSB induction, we found that depletion of factors leading to cell cycle arrest
110 also blocked transcriptional inhibition.
111
112 **Results**
113 ***HIRA independent transcriptional inhibition and recovery after ionizing radiation***
114 To detect bulk changes in nascent transcripts after irradiation *in situ*, we added the uridine analog
115 ethynyl uridine (EU) to human U2OS cells for 30 minutes. The incorporated EU was detected by
116 click chemistry to a fluorescent azide followed by immunofluorescence microscopy (Jao and Salic,
117 2008). A reduction in bulk nascent transcripts was apparent 30 minutes after exposure to 10 Gray
118 ionizing radiation (IR), and the transcriptional recovery was already occurring two hours after
119 irradiation (Fig. 1A). Co-immunofluorescence with γH2AX showed that the DNA damage signal
120 was greatly reduced at the same time point after IR where transcriptional recovery occurred (Supp.
121 Fig. 1), consistent with transcriptional recovery occurring after DSB repair. Given that the histone
122 variant H3.3 histone chaperone HIRA promotes transcriptional recovery after UV repair (Bouvier
123 et al., 2021, Adam et al., 2013), we tested whether that was also the case for transcriptional
124 recovery after IR. We found that shRNA depletion of HIRA (Supp. Fig. 2) had no effect on
125 transcriptional inhibition nor recovery after IR (Fig. 1A). In agreement, depletion of transcripts
126 encoded from both H3.3 genes (Supp. Fig. 2) had no effect on transcriptional inhibition or
127 transcriptional recovery after IR (Fig. 1B). As such, the requirement for HIRA for transcriptional
128 recovery differs following IR and UV exposure, suggesting differences in the mechanism of these
129 processes.
130

131 ***Establishment of a flow cytometry-based assay for transcriptional inhibition and recovery after***
132 ***irradiation***

133 Given that the read out of nascent EU labelled transcripts after irradiation is fluorescence, we
134 established a flow cytometry-based assay to allow us to screen for factors regulating transcriptional
135 inhibition and recovery after IR. We established this assay in a murine Abelson virus transformed
136 pre-B cell line (termed Abl pre-B cells) (Bredemeyer et al., 2006) which are non-adherent and are
137 stably transformed with doxycycline inducible Cas9 (Chen et al., 2021). By flow cytometry
138 analysis, effective incorporation of EU into nascent transcripts was apparent in a manner
139 dependent on ongoing transcription because it was inhibited by the global RNA polymerase
140 inhibitor Actinomycin D (Fig. 2A). The EU signal had 2 peaks (Fig. 2A) and we asked whether
141 this reflects cell cycle differences in the cells with higher and lower EU incorporation into the
142 nascent transcripts. We conducted cell cycle analysis by labeling newly synthesized DNA with
143 BrdU and staining DNA contents with FxCycle Violet at the same time as using EU to label
144 nascent transcripts. It was apparent that the peak with less EU was from the $G_1$ phase cells, while
145 the peak with more EU was derived from S and $G_2$ phase cells (Fig. 2B). To determine whether
146 there was a detectable reduction in EU incorporation by flow cytometry after irradiation, we
147 irradiated cells, waited different lengths of times before EU labelling of nascent RNA (Fig. 2C).
148 The transcriptional inhibition after irradiation was clearly detectable by flow cytometry as early as
149 15 minutes after IR, while transcriptional recovery was complete by 4 hours after IR (Fig. 2D).
150 Also, the extent of transcriptional repression was similar regardless of whether the IR dose was 2,
151 5 or 10 Gray (Fig. 2D, Supp. Fig. 3), suggesting that most of the reduction of nascent transcripts
152 after IR is a programmed / signaling response rather than due to proximity of the genes to the DSB,
153 which would have led to a dose response.

154

155 ***Bulk reduction of nascent transcripts after IR is mainly due to a decrease in rDNA and histone***
156 ***gene transcription***

157 To gain a better understanding of transcriptional inhibition after IR, we sought to identify the genes
158 whose transcription was being inhibited after IR. We isolated EU labelled nascent total RNA
159 transcripts 30 minutes after IR and prior to IR from two independent experiments (Supp. Fig. 4)
160 and sequenced the EU-RNA with included ERCC spike-in controls for normalization (Fig. 3A).
161 We observed that the total read count of nascent transcripts declined after IR (Fig. 3B). Most of
162 the read counts were due to rDNA transcripts, and the decline in bulk transcripts after IR was
163 mostly due to a significant decline in rDNA transcripts (Fig. 3B, Supp. Fig. 5A). By contrast, the
164 total read count from the protein coding transcripts significantly increased after IR (Fig. 3B).
165 Analysis of the protein coding transcripts showed that the transcripts of 3,026 and 1,388 protein-
166 coding genes increased and decreased after IR, respectively (Fig. 3C and 3D, Supp. Table 1). To
167 validate our EU-RNA sequencing results, we performed quantitative RT-PCR to measure the
168 nascent transcript levels of genes that were up- and down-regulated after IR. Consistently, we
169 found rDNA transcripts of *28S* and *18S* were significantly downregulated after IR; while the p53
170 regulated gene *Cyclin-dependent kinase inhibitor 1* (*Cdkn1a*/p21) was highly induced (Supp. Fig.
171 6). The gene ontology terms describing the genes that were activated after IR included known
172 DNA damage response pathways and immune related genes (Fig. 3E, Supp. Table 2). For
173 examples, the intrinsic apoptotic signaling pathway in response to DNA damage (GO:0008630),
174 type 2 immune response (GO:0042092), and cytokine-mediated signaling pathway (GO:0019221)
175 were up regulated significantly. The later may reflect immune responses triggered by cytosolic
176 DNA in the pre-B cells. Meanwhile many of the genes that were downregulated after IR included

177 gene products that are involved in chromatin organization and nucleosome assembly (Fig. 3E,
178 Supp. Table 3). For examples, chromatin silencing (GO:0006342), DNA packaging (GO:0006323),
179 and nucleosome assembly (GO:0006334) genes were down regulated significantly.
180
181 To gain more insights on how the transcription of protein coding genes was regulated after IR, we
182 defined differentially expressed genes (DEGs) between samples before and after IR. We found
183 read number from these DEGs became significantly greater after IR (Fig. 4A). We sorted the
184 protein-coding DEGs by average expression level of each gene in all 4 samples: two replicate
185 samples before IR and two replicates after IR. The number of reads derived from the mostly highly
186 expressed protein-coding DEGs became significantly smaller after IR (Fig. 4A, 4B). If the gene
187 repression after IR is due to their being *in cis* to the DNA lesion, it would be expected that genes
188 that were repressed after IR would tend to be longer, because they would be more likely to be
189 damaged. However, this was not the case because the length of the nascent transcripts was
190 equivalent regardless of whether their transcription was repressed, activated, or not changed after
191 IR (Fig. 4C). Intriguingly, we found that the repressed genes of the top 100 high-expression DEGs
192 tended to be shorter (Fig. 4C). Next, we inspected the expression level of individual protein-coding
193 genes and confirmed that most changes in gene expression after IR tended to occur for the genes
194 that were activated after IR, while many of the genes that had a high-expression level were
195 repressed after IR, for example, the histone encoding genes (Fig. 4D). Strikingly, we found that
196 vast majority of the histone genes showed reduced transcription after IR (Fig. 4E, Supp. Fig. 5B),
197 and was validated by RT-PCR analysis (Supp. Fig. 6). Finally, To determine whether
198 transcriptional repression was occurring at the initiation, elongation or both stages of transcription,
199 we examined the read counts throughout the open reading frames of the repressed protein coding

200 genes, before and after IR. We found that the decrease of transcripts mainly occurred in the gene
201 body of these genes with similar intensity at both the 3' and 5' ends of the gene body, which
202 indicates transcriptional repression after IR occurred at the initiation stage of transcription (Fig.
203 4F). Therefore, these data indicate that the bulk reduction in nascent transcripts after IR is mainly
204 due to reduced transcriptional initiation of the rDNA and histone genes.
205
206 ***A CRISPR-Cas9 screen identifies ATM, neddylation and CUL4B as promoting transcriptional***
207 ***inhibition after IR***
208 We performed a genome-wide gRNA library CRISPR-Cas9 screen in Abl pre-B cells, allowing 7
209 days for the gRNAs to inactivate their target genes (Fig. 5A). We then sorted the 10% of the cells
210 with the most nascent RNA (high EU) 30 minutes after IR, as these would include cells with
211 gRNAs corresponding to gene products that are required for transcriptional inhibition after IR. We
212 sequenced the gRNAs within the high EU cells and within the total cell population. We calculated
213 an enrichment score for each of the 5 gRNAs that were included in the library against each gene
214 (Supp. Table 4, Supp. Fig. 7). Fig. 5B shows the enrichment scores for the 5 gRNAs for some of
215 the top hits (high EU) from the screen. We found that gRNAs against ATM were enriched in the
216 high EU cells, consistent with the fact that transcriptional inhibition of a gene after induction of a
217 DSB requires ATM signaling (Shanbhag et al., 2010). Other top hits included most of the
218 machinery that mediates neddylation, the post translational covalent addition of NEDD8, a small
219 ubiquitin-like peptide, onto other proteins (Rabut and Peter, 2008). These hits included the *Nedd8*
220 gene encoding the NEDD8 ubiquitin like modifier, *Nae1* encoding NEDD8 activating enzyme E1
221 subunit 1 NAE1, *Uba3* encoding the Ubiquitin like modifier activating enzyme 3 UBA3,
222 *Ube2m/Ubc12* encoding the NEDD8-conjugating enzyme UBC12, *Ube2f* encoding a neddylation

223 E2 enzyme UBE2F, and *Rbx1* and *Rbx2* which encode linkers that facilitate NEDD8 transfer from
224 the E2 enzyme to Cullins (Fig. 5B). We also uncovered gRNAs against the gene encoding the
225 neddylation substrate CUL4B enriched in the high EC cells (Fig. 5B). These data suggested that
226 neddylation may have a novel role in transcriptional inhibition after IR.
227
228 We validated the role of ATM in bulk transcriptional inhibition after IR with the ATM inhibitor
229 Ku55933 (Fig. 5C). To validate a role for neddylation in transcriptional shut off after IR, we
230 depleted NAE1 with a gRNA to *Nae1* (Supp. Fig. 8) and showed that NAE1 also greatly reduced
231 transcriptional inhibition after IR (Fig. 5D). Similarly, a 16-hour treatment with the neddylation
232 inhibitor MLN4924 also greatly reduced transcriptional inhibition after IR (Fig. 5E). To ensure
233 that the role of neddylation in transcriptional inhibition after IR is not unique to the murine Abl
234 pre-B cells, we found that transcriptional inhibition, detected by fluorescence microscopy, in
235 U2OS cells was significantly reduced upon inhibition of neddylation (Fig. 5F). As such, these data
236 suggest that neddylation is required for efficient transcriptional inhibition after IR.
237
238 While most neddylation substrates have only been identified upon overexpression of the
239 neddylation machinery, the Cullins have been shown to be *bone fide* neddylation substrates *in vivo*
240 (Pan et al., 2004). Given that we found gRNAs to Cul4b encoding CULLIN 4B enriched in the EU
241 high cells (Fig. 5B) we asked whether its neddylation is induced after IR. We found that when
242 compared to the level of unneddylated CUL4A there was not a significantly higher proportion of
243 neddylated CUL4A or CUL4B in U2OS cells after IR (Fig. 6A). We used the neddylation inhibitor
244 MLN4924 as a positive control to confirm which bands were neddylated CUL4A and CUL4B
245 (Fig. 6A). To determine whether CUL4B or CUL4A were required for IR induced transcriptional

246 inhibition, we made stable Abl pre-B cell lines lacking each protein by gRNA-mediated disruption
247 of the *Cul4a* or *Cul4b* genes. Loss of CUL4A had no effect on transcriptional inhibition after IR,
248 while loss of CUL4B partially reduced transcriptional inhibition after IR (Fig. 6B, Supp. Fig. 9A).
249 Given that CUL4B and CUL4A show some functional redundancy (Hannah and Zhou, 2015,
250 Brown et al., 2015), we depleted both proteins at the same time. Additional transient bulk gRNA
251 transfection-mediated depletion of CUL4A from cells lacking CUL4B (depletion of both CUL4A
252 and CUL4B is lethal) did not further increase the block of transcriptional inhibition after IR (Supp.
253 Fig. 9B). As such, these data indicate that CUL4B but not CUL4A contributes to transcriptional
254 inhibition after IR. Given that neddylation of CUL4A/CUL4B regulates cell cycle progression
255 (Hannah and Zhou, 2015), and we saw changes in the distribution of the cell cycle phases upon
256 CUL4A/CUL4B depletion and upon blocking neddylation as indicated by the change in relative
257 heights of the EU low ($G_1$) and EU high ($S/G_2$) peaks (Fig. 5D, 5E, 6B and Supp. Fig. 9B, 9C), we
258 wondered if cell cycle arrest may be influencing transcriptional inhibition after IR. Accordingly,
259 we inhibited neddylation for 1-3 hours in Abl pre-B cells, which effectively inhibited neddylation
260 (Fig. 6C) and tested the effect on transcriptional inhibition after IR. Strikingly, we observed
261 transcriptional inhibition after IR even upon neddylation inhibition treatment for 1-3 hours (Fig.
262 6D), indicating that neddylation is not required for transcriptional inhibition after IR. We also
263 observed that the length of time required for treatment with the neddylation inhibition to block
264 transcriptional inhibition after IR (Fig. 5E) caused arrest of the cell cycle in $G_2$ phase (Supp. Fig.
265 10). Therefore, these data indicate that neddylation *per se* is not required for transcriptional
266 inhibition after IR. They also raise the possibility that the cell cycle arrest caused by persistent loss
267 of neddylation may prevent transcriptional inhibition after IR.
268

269 ***Cell cycle arrest in $G_1$ or $G_2$ phase blocks inhibition of transcription after IR***

270 To directly determine the relationship between cell cycle arrest caused by prolonged neddylation
271 inhibition and transcriptional inhibition after IR, we labelled the Abl pre-B cells with both EU
272 (nascent transcripts) and 7-Aminoactinomycin D (7-AAD) (DNA stain). Prolonged neddylation
273 inhibition led to accumulation of cells with a 4N DNA content and greatly reduced transcriptional
274 inhibition after IR (Fig. 7A, Supp. Fig. 10). To investigate if this correlation was specific to
275 neddylation inhibition, we used an unrelated inhibitor that causes cell cycle arrest with a 4N DNA
276 content, RO-3306, a CDK1 inhibitor (Vassilev et al., 2006). We also saw accumulation of cells
277 with a 4N DNA content and no transcriptional inhibition after IR upon CDK1 inhibition (Fig. 7B,
278 Supp. Fig. 10). To determine whether this effect was unique to cells arrested with a 4N DNA
279 content or was shared with conditions that cause arrest in $G_1$ phase, we treated cells with 10% or
280 0.1% FBS, where the later lead to arrest in $G_1$ phase (due to serum depletion) and prevented
281 transcriptional inhibition after IR (Fig. 7C). It is relevant to point out that the level of bulk nascent
282 transcripts in cells arrested in $G_1$ by serum depletion is still far higher than cells lacking EU (Fig.
283 7C), suggesting that the limited transcriptional inhibition after IR in $G_1$ arrested cells is not just
284 because there is only minimal transcription occurring. In agreement, two CDK4/6 inhibitors,
285 Ribociclib and Palbociclib, that lead to $G_1$ arrest also prevented transcriptional inhibition after IR
286 (Fig. 7D, 7E). Intriguingly, these data indicate that multiple different treatments that lead to cell
287 cycle arrest in $G_1$ or $G_2$ *per se* prevent transcriptional inhibition after IR.

288

289 To gain molecular insight into why ATM-dependent bulk transcriptional inhibition occurs after IR
290 in cycling cells but not in arrested cells, we investigated the possibility that ATM-dependent
291 pathways that inhibit rDNA transcription after IR in cycling cells (Kruhlak et al., 2007) fail in

292 arrested cells. In cycling cells, DSBs within the rDNA trigger formation of nucleolar caps due to
293 damaged rDNA and associated proteins relocalizing to the nucleolar periphery (van Sluis and
294 McStay, 2017). In cycling cells, DSBs within the rDNA trigger ATM-dependent phosphorylation
295 of Treacle which promotes recruitment of NBS1 and TOPBP1 to the nucleolar caps to inhibit
296 rDNA transcription (Larsen et al., 2014, Mooser et al., 2020). Accordingly, in cycling cells,
297 TOPBP1 accumulates in the nucleolar caps after induction of DSBs, concomitant with repression
298 of rDNA transcription (Sokka et al., 2015, Mooser et al., 2020). We asked whether TOPBP1-eGFP
299 recruitment to nucleolar caps was disrupted after DNA damage in cells arrested by treatment with
300 MLN4924 or RO-3306. The overall induction of TOPBP1 expression was not affected by inhibitor
301 treatment (Supp. Fig. 10). However, the percentage of cells with TOPBP1-eGFP localizing to
302 nucleolar caps after IR was markedly reduced upon MLN4924 and RO-3306 treatment (Fig. 7F,
303 7G). These results are consistent with arrested cells failing to repress rDNA expression after global
304 DNA damage, as a consequence of compromised ATM-dependent localization of TOPB1 to
305 nucleolar caps.
306
307 **Discussion**
308 We find that while the bulk abundance of nascent transcripts is rapidly reduced after IR, more
309 protein coding genes are induced than inhibited after IR. Instead, the reduction in bulk nascent
310 transcript levels that occurs after IR is due to reduced transcriptional initiation of a subset of genes
311 that are the most highly expressed in the cell – the rDNA and histone encoding genes. Notably,
312 bulk transcriptional inhibition after IR did not occur in cells arrested in $G_1$ or $G_2$ phases of the cell
313 cycle indicating that cells have to be cycling for IR to rapidly inhibit bulk transcription. The length-
314 independent and dose-independent reduction in bulk abundance of nascent transcript after IR (Figs.

315 5C, Supp. Fig 3) suggests that the reduced bulk abundance of nascent transcripts after IR occurs
316 *in trans* and is a programmed event. This is in contrast to studies that have found transcriptional
317 inhibition *in cis* of a gene immediately adjacent to an endonuclease-induced DSB. Our work
318 indicates that the genome wide transcriptional response to DSBs after IR cannot be extrapolated
319 from single gene studies.
320
321 Analysis of nascent transcripts at early times after irradiation revealed a different transcriptional
322 response compared to changes in total mRNAs after irradiation (Lieberman et al., 2017). These
323 changes in mRNA levels typically occurred in an IR dose-dependent manner. By contrast, the bulk
324 changes in nascent transcripts occurred in a dose-independent manner (Fig. 2D). Analysis of total
325 mRNAs changes following IR showed altered expression of genes involved in signal transduction,
326 regulation of transcription, and metabolism (Su et al., 2004). Similarly, the upregulated nascent
327 transcript changes identified pathways including signal transduction, while nascent transcripts
328 from protein-coding genes that affected nucleosome assembly and chromatin structure (histones)
329 were downregulated after IR (Fig. 3B, 3E). Finally, most of the gene expression changes detected
330 by analysis of total mRNA continued to increase or decrease over long periods of time, up to 48
331 hours (Su et al., 2004), whereas the reduction of bulk nascent transcript levels occurred in a very
332 transient manner and was already returning to normal by 4 hours after IR (Fig. 1, Fig. 2D).
333
334 How is bulk nascent transcription being inhibited after irradiation? Reminiscent of the ATM
335 dependence on the changes in mRNA levels after IR (Artuso et al., 1995), the reduction in bulk
336 nascent transcript levels after IR was also dependent on ATM (Fig. 5C). Given that most of the
337 reduction in bulk nascent transcript levels was due to the rRNA (Fig. 3B), this is consistent with

338 the previous report of ATM-dependent inhibition of RNA Polymerase I transcription in response
339 to DSBs (Kruhlak et al., 2007). In this case, the Pol I transcription appeared to be inhibited at both
340 the initiation and elongation stages (Kruhlak et al., 2007). Sequencing analysis of nascent
341 transcripts of protein-coding genes whose expression significantly decreased 30 minutes after IR
342 indicated that it is the initiation of Pol II transcription that is inhibited, given that the reduction in
343 sequencing reads at the 5' end and 3' ends of open reading frames was equivalent (Fig. 4F). Studies
344 that examined the mechanism of Pol II transcriptional inhibition of one gene adjacent to an
345 endonuclease induced DSB identified a reduction in transcriptional elongation as indicated by
346 reduced Pol II Ser2 phosphorylation (Shanbhag et al., 2010), while other studies found a defect in
347 both Pol II initiation and elongation of a different gene adjacent to an endonuclease induced DSB,
348 in a manner dependent on DNA-PK and the proteasome (Caron et al., 2019, Pankotai et al., 2012).
349 From our analysis, the major mechanism for the repression of the ~1,000 protein coding genes
350 after IR occurs at the transcriptional initiation stage.
351
352 Rapid inhibition of transcription *in cis* has been observed following endonuclease-mediated DSB
353 induction, where a DSB-proximal transcriptional reporter was inhibited while a second
354 transcriptional reporter inserted elsewhere in the genome without a proximal FokI nuclease site
355 was not inhibited after induction of Fok1 (Shanbhag et al., 2010). If the transcriptional inhibition
356 after IR that we observe was occurring *in cis,* we would expect that longer genes would be more
357 inhibited than shorter genes after IR, as they are more likely to experience a DSB induced by IR.
358 However, this was not the case because the length of the nascent transcripts was equivalent
359 regardless of whether their levels were increased, didn't change, or were decreased after IR (Fig.
360 4C). We would also expect that bulk transcript levels would be more reduced with a higher dose

361 of IR if it occurred *in cis*, but that was not the case (Fig. 2D). In fact, transcriptional repression
362 around a nuclease-induced DSB can spread hundreds of kb away from the break, throughout a
363 whole topological associated domain marked by gamma H2AX (Purman et al., 2019). Importantly,
364 our data do not contradict that DSBs can induce transcriptional inhibition *in cis*, rather it likely
365 reflects the random nature of the DNA damage induced by IR is not sufficient to detect inhibition
366 *in cis*, as every cell will have DNA DSBs at different locations. We also are examining the effect
367 following global DNA damage induced IR versus the effect of induction of a single or limited
368 numbers of DSBs by endonuclease induction. It is noteworthy that the nascent transcript levels of
369 more genes rapidly increased after IR than were reduced (Figs. 3 and 4), such that the situation, at
370 least after IR, is more complex than transcriptional inhibition *in cis* to the DSBs.
371
372 The change in transcript levels after irradiation tended to depend on the expression level of the
373 genes before irradiation. Those genes that were normally most highly transcribed were repressed
374 after IR, while genes that were normally expressed at intermediate or low levels tended to be
375 induced after IR (Fig. 4A). The mechanistic reason for this is unclear. Among the genes that were
376 most repressed after IR treatment were many of the histone encoding genes (Fig. 4D, 4E). Histone
377 gene expression has been shown to be reduced after IR previously in a manner dependent on ATM
378 and p53, as seen at the mRNA level 10 hours or more after irradiation (Su et al., 2004). By contrast,
379 reduction in nascent histone transcript levels occurred 30 mins after IR (Fig. 4D, 4E). Interestingly,
380 we observed a tremendous expression induction of *Cdkn1a/p21* gene, which encodes a potent
381 cyclin-dependent kinase inhibitor, after IR (Supp Fig. 6). The histone transcriptional coactivator
382 NPAT induces histone transcription when it is phosphorylated by cyclin E/CDK2 (Zhao et al.,
383 1998, Zhao et al., 2000, Ma et al., 2000). As such, highly elevated levels of Cdkn1a/p21 after IR

384 might inactivate cyclin E/CDK2, leading to hypo-phosphorylation of NPAT and an immediate
385 repression of histone gene expression after IR.
386
387 In response to UV exposure, bulk inhibition of transcription occurs, followed by transcriptional
388 recovery after repair of UV-induced damage, where transcriptional recovery after repair of UV-
389 induced damage is dependent on the histone variant H3.3 histone chaperone HIRA (Bouvier et al.,
390 2021, Adam et al., 2013). Mechanistically, HIRA functioned to repress the transcriptional
391 repressor ATF3, in turn promoting transcriptional recovery after repair of UV-induced damage
392 (Bouvier et al., 2021). We find that neither HIRA nor H3.3 is required for recovery of bulk nascent
393 transcripts after DSB repair (Fig. 1). Additionally, we find that the genes that have altered levels
394 of nascent transcripts after UV damage (Bouvier et al., 2021) and after IR are quite distinct (data
395 not shown). However, the UV studies were performed on nascent mRNA from a human cell line,
396 while our studies were performed on total nascent RNA from a mouse cell line.
397
398 Why didn't our CRISRP/Cas9 screen of factors responsible for bulk nascent transcript inhibition
399 after IR identify previously reported factors involved in Pol II transcriptional inhibition proximal
400 to an endonuclease-induced DSB? This is likely because most of the reduction in bulk nascent
401 transcript level that we were detecting after IR was due mainly to reduced transcript abundance
402 from the rDNA, rather than Pol II transcripts (Fig. 3B). We did find ATM in the screen (Fig. 5B,
403 5C), and this is consistent with the fact that ATM is required for rDNA transcriptional inhibition
404 after IR (Kruhlak et al., 2007). Many of the most significant hits from the screen encoded factors
405 that are involved in the neddylation pathway and the neddylation substrate CUL4B (Fig. 5D, 5E,
406 5F and Fig. 6B). However, short times of neddylation inhibition were sufficient to inhibit

407 neddylation but did not prevent transcriptional inhibition after IR (Fig. 6C, 6D). Longer times of
408 neddylation inhibition did prevent transcriptional inhibition after IR (Fig. 5E, 5F), but also caused
409 cell cycle arrest (Fig. 7A, Supp. Fig. 10). These results lead us to speculate that neddylation is not
410 directly involved in transcriptional inhibition after IR, but that neddylation promotes cell cycle
411 progression, and that it is the cell cycle arrest occurring upon neddylation inhibition that prevents
412 the bulk reduction of nascent transcript levels after IR. Consistent with cell cycle arrest *per se*
413 preventing transcriptional inhibition after IR, we also found that CDK1 inhibition leading to $G_2$
414 arrest, and serum starvation and CDK4/6 inhibition leading to $G_1$ arrest, also prevented bulk
415 transcriptional inhibition after IR (Fig. 7). Indeed, transcription of rDNA is known to be reduced
416 when in non-cycling cells when total transcript levels were measured (Moss and Stefanovsky,
417 1995, O'Mahony et al., 1992) while transcription of histone genes requires ongoing DNA
418 replication (Sittman et al., 1983). As such, one possibility for failure to see bulk reduction in
419 nascent transcript abundance after IR in arrested cells may be that rDNA and histone transcription
420 is already reduced in $G_1$ and $G_2$ arrested cells. However, we found that the total level of bulk
421 nascent transcripts during $G_2$ arrest before IR were equivalent to, or more than, the level of bulk
422 nascent transcripts before cell cycle arrest (compare grey (no arrest) to black lines (cell cycle
423 arrest) in Figs. 5C-E, 7A, 7B) which suggest that the levels of rDNA transcripts may not be reduced
424 during $G_2$ arrest given that most of the nascent transcripts are from the rDNA in the conditions of
425 our experiments (Fig. 7B). It is also possible that a factor that is required for transcriptional
426 inhibition of the rDNA after IR is absent or inactive in arrested cells.
427
428 In addition to ATM, NBS1 was previously shown to be required for transcriptional inhibition of
429 rDNA after IR (Kruhlak et al., 2007). The mechanism for this was unclear, but it is tempting to

430 speculate that the requirement of ATM for transcriptional inhibition after IR in cycling cells may
431 be mediated through ATM-dependent phosphorylation of Treacle. In this form, Treacle functions
432 with TOPBP1 to promote recruitment of NBS1 to nucleolar caps to repress rDNA transcription
433 (Larsen et al., 2014, Mooser et al., 2020). That TOPB1 fails to relocalize to nucleolar caps after
434 IR in arrested cells (Fig. 7F, 7G) is consistent with a potential loss of ATM-dependent treacle
435 phosphorylation in arrested cells, which would prevent reduction in rDNA transcription after DNA
436 damage. Future experiments will reveal further insight into the cell cycle dependent control of
437 transcriptional inhibition of highly transcribed genes after DNA damage.
438

439 ## Figure legends

440 **Figure 1. Transcriptional inhibition after irradiation and transcriptional restart after DNA**
441 **repair in a HIRA independent manner. A.** U2OS cells were transfected with either a scrambled
442 shRNA or shRNA against HIRA, and were either incubated with EU or not, as indicated, and were
443 irradiated (10 Gy) or not as indicated, followed by detection of EU by click chemistry of a
444 fluorophore and DNA was detected by DAPI staining. The right panel shows quantitation of the
445 mean intensity of EU in at least 80 cells for each condition. **** indicates $p<0.001$, ** indicates
446 $p<0.01$, by students T-test. **B.** U2OS cells were transfected with either a control siRNA (siRNA-
447 Ctrl) or two siRNAs against each gene encoding H3.3 (siRNA-H3). EU and DAPI were detected
448 as described in A and quantitated as described in A. **** indicates $p<0.001$, *** indicates
449 $p<0.005$, * indicates $p<0.05$ by students T-test.
450

451 **Figure 2**. **Development of a flow cytometry assay for nascent transcripts shows that**
452 **transcriptional inhibition after IR is not dose dependent. A.** The EU positive signal in murine

453 Abl pre-B cells detected by flow cytometry is due to transcripts, as indicated by the addition of
454 5μM of the general RNA polymerase inhibitor Actinomycin D for 1 hour. **B**. The two EU peaks
455 observed by flow cytometry correspond to $G_1$ (low peak) and $G_2$ (high peak) cells. Cycling Abl
456 pre-B cells (left panel) were gated for those with 2N DNA ($G_1$) content or 4N ($G_2$) content as
457 detected by FxCycle Violate or with BrdU incorporation (S) as indicated and were individually
458 analyzed for EU incorporation into nascent transcripts (right panel). **C.** Schematic of the assay to
459 detect transcriptional inhibition and transcriptional recovery after IR. **D.** Time course of
460 transcriptional inhibition and recovery in Abl pre-B cells after IR with the indicated times after IR
461 at the indicated doses of IR.
462
463 **Figure 3. Reduction of nascent transcript levels after irradiation is mainly of the rDNA.**
464 **A.** Schematic of nascent transcript sequencing. **B.** Read counts for the total nascent transcripts,
465 rDNA transcripts and protein coding transcripts before and 30 minutes after IR, normalized to
466 ERCC spike in controls. **C**. Significantly changed nascent transcripts from protein coding genes
467 are indicated upon irradiation, and the numbers indicate the number of upregulated and
468 downregulated genes 30 minutes after IR. Data shown are an average of the two independent
469 experimental repeats. **D.** Heat map of significantly increased and decreased nascent transcripts 30
470 minutes after IR, shown for two independent experimental repeats. Expression z-score was
471 calculated by subtracting the overall average gene abundance from the raw expression for each
472 gene and dividing that result by the standard deviation (SD) of all of the measured counts across
473 all samples. **E.** Gene Ontology analysis of the top significantly enriched GO terms most
474 upregulated after IR (pink) and most downregulated after IR (blue). Enriched gene number (red)
475 and fold enrichment (blue) were showed in each GO term.

476

477 **Figure 4. The highly transcribed protein coding genes tend to be repressed after irradiation,**
478 **due to a decrease in the transcription of the histone genes. A.** Plot of the transcript abundance
479 of differentially expressed genes (DEGs) showing that highly expressed genes have reduced
480 nascent transcript levels 30 minutes after IR, while moderately expressed and low level expressed
481 genes tend to have increased nascent transcript levels 30 minutes after IR. Mean gene expression
482 and standard deviation is shown in million reads mapped to genes normalized by ERCC spike-in
483 reads. Data are shown from two independent experimental repeats (rep) of the experiment. **B.** Heat
484 map showing nascent transcript levels of the top 100 highly expressed DEGs, ranked by gene
485 expression from top (highest) to bottom, 30 minutes after IR, shown for two independent
486 experimental repeats. Expression z-score was calculated by subtracting the overall average gene
487 abundance from the raw expression for each gene and dividing that result by the standard deviation
488 (SD) of all the measured counts across all four samples. **C.** Among the top 100 of highly expressed
489 protein-coding genes, repressed genes are significantly shorter compared to activated genes. The
490 activated, non-changed and repressed genes show little difference in gene size (the data are
491 averaged for each gene between two independent experimental repeats). **D.** Plot of change in gene
492 expression after IR against mean gene expression ($log_2$), ranked by mean gene expression in
493 samples before IR on the x axis, for all nascent transcripts. Some of the highly expressed genes
494 whose nascent transcript levels decreased after IR are labelled in the rectangle, including histone
495 genes. **E.** Heat map of nascent transcripts of all histone genes 30 minutes after IR, shown for two
496 independent experimental repeats. **F**. The average read counts for repressed protein coding genes
497 throughout their gene length before and after IR for 2 independent repeats of the experiment.
498

499 **Figure 5. Whole genome gRNA screen CRISPR-Cas9 screen for factors involved in**
500 **transcriptional inhibition after irradiation identifies the neddylation pathway. A.** Schematic
501 of whole genome gRNA CRISPR-Cas9 screen for gene products that promote transcriptional
502 inhibition after IR**. B.** Fold enrichment of 5 guide RNAs against the indicated genes in the 10% of
503 cells with most EU incorporated into transcripts 30 minutes after IR. **C**. Inhibition of ATM greatly
504 reduces transcriptional inhibition 30 minutes after IR in Abl pre-B cells. The inhibitor was used at
505 15 μM for 1 hours. **D.** gRNA mediated depletion of Nae1 greatly reduces transcriptional inhibition
506 30 minutes after IR in Abl pre-B cells. **E.** Inhibition of neddylation greatly reduces transcriptional
507 inhibition 30 minutes after IR. The inhibitor was used at 1μM for 16 hours in Abl pre-B cells. **F.**
508 Inhibition of neddylation reduces transcriptional inhibition after IR in U2OS cells, as detected by
509 fluorescence analysis of nascent transcripts as described in legend to Fig. 1 and quantitated as in
510 Fig. 1. Significant difference after IR compared to before IR are indicated by asterisks, where ****
511 indicates $p<0.001$, * indicates $p<0.05$ by students T-test. All experiments in this figure are in
512 murine Abl pre-B cells.
513
514 **Figure 6. CUL4B but not CUL4A contributes to transcriptional inhibition after irradiation.**
515 **A.** Analysis of CUL4A and CUL4B neddylation in U2OS cells after IR, in the absence of presence
516 of 10 μM treatment for 3 hours with the neddylation inhibitor. N8 indicates the neddylated species.
517 **B.** Analysis of nascent transcripts in Abl pre-B cell lines stably depleted of CUL4A or CUL4B 30
518 minutes after IR, as indicated. **C.** Short treatment of Abl pre-B cells with neddylation inhibitor
519 MLN4924 is sufficient to block neddylation of CUL4B. **D.** The same cells used in C were analyzed
520 for EU incorporation into nascent transcripts 30 minutes after irradiation, without or with the
521 indicated time of MLN4924 treatment before irradiation.

522

523 **Figure 7. Cell cycle arrest in $G_1$ or $G_2$ prevents transcriptional inhibition after DNA damage.**
524 **A.** Abl pre-B cells were treated with MLN4924 (1 μM) for 16 hours, followed by IR and staining
525 of DNA with 7-AAD and nascent transcripts with EU 30 minutes after IR. **B.** Abl pre-B cells were
526 treated with RO-3306 (10 μM) for 16 hours, followed by IR and staining of DNA with 7-AAD and
527 nascent transcripts with EU 30 minutes after IR. **C.** The left two panels show the cell cycle
528 distribution of Abl pre-B cells after growth for 72 hours in 1% FBS or 0.1% FBS. The rectangles
529 and numbers indicate the % of cells with a 2N DNA content. The right panel shows the EU
530 incorporated into nascent transcripts 30 minutes after IR for the same samples. **D.** Abl pre-B cells
531 were treated with Ribociclib (5 μM) for 24 hr., followed by IR and staining of DNA with 7-AAD
532 and nascent transcripts with EU 30 minutes after IR. **E.** Abl pre-B cells were treated with
533 Palbociclib (5 μM) for 24 hr, followed by IR and staining of DNA with 7-AAD and nascent
534 transcripts with EU 30 minutes after IR. **F.** The U2OS cells were treated with doxycycline (1
535 μg/mL) for 12 hours to express eGFP-TOPBP1. Then, DMSO, MLN4924 and RO3306 were added
536 to the cells for another 16 hours. TOPBP1 localization was shown in cells before IR or 2 hours
537 after IR (10 Gy). Scale bar is 10 μm. **G.** Quantification of TOPBP1 expressing cells with nucleolar
538 caps before and after IR (10 Gy) in cells treated with MLN4924 and RO-3306. Data shown are an
539 average of the three independent experimental repeats. Significant differences are indicated by
540 asterisks, where ** indicates $p<0.01$ by students T-test.

541

542 **Supplementary Figure 1. Transcriptional inhibition after irradiation and transcriptional**
543 **restart after DNA repair in U2OS cells. A.** U2OS cells were either incubated with EU or not, as
544 indicated, and were irradiated (10 Gy) or not as indicated, followed by detection of the EU by click

545 chemistry of a fluorophore, and immunofluorescence staining of gamma H2AX in the same cells
546 and the DNA was detected by Hoechst staining.
547
548 **Supplementary Figure 2. Confirmation of knockdown of HIRA and H3.3**. The samples were
549 from the same experiments shown in Figure 1.
550
551 **Supplementary Figure 3. The mean intensities of the EU peaks shown in Figure 2D are**
552 **indicated.** The mean value of each sample was calculated by Flowjo software.
553
554 **Supplementary Figure 4. Nascent transcript levels before and after 30 minutes of IR.** The
555 samples from two independent experiments were used for the EU-seq and analyses in Fig. 3 and
556 4.
557
558 **Supplementary Figure 5. Screen shot from the UCSC browser of nascent transcripts. A.**
559 Nascent transcripts before and after IR over ribosomal DNA (rDNA). **B.** Nascent histone
560 transcripts before and after IR over histone cluster 1.
561
562 **Supplementary Figure 6. Validation of nascent transcript levels of DEGs from EU-RNA seq**
563 **by real-time quantitative RT-PCR.** Samples from three independent experiments were used for
564 the analyses. Ct value is presented to show the absolute amounts of EU labeled RNA transcripts
565 from the same number of cells before and after 30 minutes of IR (10 gray). Significant difference
566 after IR compared to before IR are indicated by asterisks, where ** indicates $p < 0.01$, * indicates
567 $p < 0.05$ and ns indicates non-significant by students T-test.

568

569 **Supplementary Figure 7. CRISPR-Cas9 screen identifies genes promoting transcriptional**
570 **inhibition after IR.** A volcano plot of guide RNA changes between Eu high cells and unsorted
571 cells. Labeled genes are some of those that have P adjust <= $10^{-6}$.

572

573 **Supplementary Figure 8. Confirmation of knockdown of Nae1.** gEV is an empty vector. The
574 samples were from the same experiments shown in Figure 5D.

575

576 **Supplementary Figure 9. Analysis of CUL4A and CUL4B depletion. A.** The western blot
577 shows the CUL4A and CUL4B levels from the experiment shown in Fig. 6B. Additionally gRNAs
578 were used to deplete CUL4A in cul4b cells and CUL4B in cul4a cells and their western blot
579 analyses are also shown. **B.** The EU analysis of these double depleted cells is shown**. C.** Cell cycle
580 analysis of the experiment shown in A and B and Fig. 6B.

581

582 **Supplementary Figure 10. Cell cycle analysis of cells treated with MLN4924 and RO3306**.
583 MLN4924 or RO3306 treatment leads cell cycle arrest in $G_2$ phase. **B.** Quantification of cells with
584 TOPBP1 expression before and after IR (10 Gy) in cells treated with MLN4924 and RO-3306.
585 The samples were from the same experiments shown in Fig. 7F, 7G.

586

587 **Supplementary Table 1.** Nascent RNA profiles of each gene using EU RNA-seq.

588

589 **Supplementary Table 2.** Significantly enriched GO terms for up-regulated gene after irradiation.

590

591 **Supplementary Table 3.** Significantly enriched GO terms for down-regulated genes after
592 irradiation.
593
594 **Supplementary Table 4.** Whole genome CRISPR-Cas9 screen detects the abundance of all
595 gRNAs and target genes for EU high cells and unsorted cells.
596

597 ## Methods and materials

598 **Cell culture and transfections**

599 U2OS cells (ATCC, HTB-96) were cultured in McCoy's 5A (Corning, 10050CV) medium
600 supplemented with 10% fetal bovine serum (FBS) and 1% Penicillin-Streptomycin. Abelson virus-
601 transformed pre-B cells were maintained in DMEM (Thermo Fisher, 11960-077) supplemented
602 with 10% FBS, 1% Penicillin-Streptomycin, 1x nonessential amino acids, 1 mM sodium pyruvate,
603 2 mM L-glutamine, and 0.4% beta-mercaptoethanol. HEK-293T cells were maintained in DMEM
604 (Corning, 10-013-CM) supplemented with 10% FBS and 1% Penicillin-Streptomycin. All the cells
605 were grown at 37 °C under a humidified atmosphere with 5% CO2.
606 SiRNA oligos against human H3F3A and H3F3B (SMARTPool) for RNAi in U2OS cells were
607 purchased from Horizon Discovery (Dharmacon). 100 nM of H3F3A and H3F3B were mixed with
608 Lipofectamine RNAiMAX transfection reagent (Thermo Scientific, 13778150) according to the
609 manufacturer's protocol to knockdown H3.3 for 48 hours. The siRNA control (ON-TARGETplus
610 non-targeting) was also purchased from Horizon Discovery (Dharmacon) and used as negative
611 control. shRNA lentiviral plasmids against HIRA (5'-TAGAGCATACCAAGATGCC-3') and the
612 control were described in a previous study (Huang et al., 2018). HEK-293T cells were transfected
613 with a mixture of shRNA plasmids and the viral packaging and envelope vectors, pCMV-dR8.2

614 and pCMV-VSVG. The media containing shRNA virus particles were collected 48 to 72 hours
615 after transfection and filtered through a 0.45 μm filter. Cells were incubated with the lentiviral
616 supernatant containing 5 μg/ml polybrene (Sigma-Aldrich, S2667) for 24 hours, followed by 1
617 μg/mL Puromycin selection for another 48 hours. To inactivate Nae1, Cul4a and Cul4b in bulk
618 cell populations, guide RNAs (gRNAs) against each gene were cloned into pKLV-U6gRNA-
619 EF(BbsI)-PGKpuro2ABFP (Addgene, #62348) modified to express human CD2 or Thy1.1 as cell
620 surface markers. The pKLV-gRNAs lentiviruses were prepared in 293T cells as described above.
621 The Abl pre-B cells containing pCW-Cas9 (addgene, #50661), which can express Cas9 with
622 doxycycline induction, were mixed with viral supernatant supplemented with 5 μg/ml polybrene
623 and centrifuged at 1800 rpm for 1.5 hours at room temperature. After the spin-infection, the
624 transduced cells were maintained in DMEM with 3 μg/ml doxycycline (Sigma-Aldrich, D9891)
625 for 3 days before flow cytometric cell sorting based on hCD2 or Thy1.1 expression. To make stable
626 cell lines depleted of Cul4a and Cul4b, serial dilution of the sorted cells into 96-well plate was
627 used to isolate single cells. Western blot analysis was used to determine the knockdown efficiency
628 of each target genes.
629 In EU flow cytometric and immunofluorescence analysis, final concentrations of 15 μM ATM
630 inhibitor Ku55933 (Selleck Chemicals, S1092) and 5 μM of Actinomycin D (Sigma-Aldrich,
631 A9415) were added to cell culture 1 hour prior to irradiation. 1 μM and 10 μM of neddylation
632 inhibitor MLN4924/Pevonedistat (Active Biochem, A-1139) were used for long (16 hours) and
633 short (1 to 3 hour) treatments, respectively. To arrest cells in $G_1$ cell cycle phase, cells were
634 incubated in media supplemented with 5 μM Palbociclib (Selleck Chemicals, S1116) or 5 μM
635 Ribociclib (Selleck Chemicals, S7440) for 24 hours. For serum starvation, Abl pre-B cells were
636 grown in complete medium containing 10% of FBS to desired density and collected and washed

637 in medium with reduced concentration (0.1%) of FBS. The cells were maintained in the medium
638 with reduced FBS for 72 hours to arrest in $G_1$ phase. Representative data are shown for experiments
639 repeated three of more times with consistent results.
640
641 **Western blots**
642 The following antibodies were used for western blot: CUL4A (Cell Signaling Technology, 2699S,
643 1:1000), CUL4B (Proteintech, 12916-1-AP, 1:1000), H3.3 (Millipore Sigma, 09-838, 1:1000),
644 HIRA (Abcam, ab20655, 1:1000), NAE1 (Thermo Fisher, PA5-59836, 1:500), GAPDH (Sigma-
645 Aldrich, G8795, 1:5000). Representative data are shown for experiments repeated three of more
646 times with consistent results.
647
648 **Fluorescence microscopy**
649 For immunofluorescence, Click-iT RNA Alexa Fluor Imaging Kit (Thermo Fisher, C10330) was
650 used to label newly synthesized RNAs in the cells. Briefly, 50,000 U2OS cells grown on cover
651 slips in 24-well plate were irradiated with 10 Gray and allowed to recover for indicated times at
652 37°C with 5% CO2. 0.5 mM EU was added to the medium and incubated for 45 minutes for EU
653 incorporation. Cells were then washed with PBS, fixed in 4% paraformaldehyde PBS for 15
654 minutes at room temperature, and permeabilized in cold 0.5% Triton X-100 PBS for 10 minutes.
655 Cells were blocked in 3% BSA-PBS for 1 hour at room temperature and subsequently incubated
656 overnight at 4 °C in primary antibody (anti-γH2AX (S139), EMD Millipore, 05-636). Coverslips
657 were then washed 3x with PBST (0.05% Tween 20), incubated with secondary antibody diluted in
658 3% BSA PBS (Alexa Fluor 488 Goat anti-mouse IgG, BioLegend, 405319) in the dark for 1 hour
659 at room temperature and washed 3x with PBST. Click-iT reaction cocktail was prepared according

660 to the manufacturer's protocol and immediately added to the cells to perform click reaction in the
661 dark for 30 minutes at room temperature. After washes with Click-iT reaction rinse buffer
662 (Component F) and PBS, cells were stained with Hoechst (1:2000) or DAPI (Sigma-Aldrich,
663 D9542) in PBS for 10 minutes and mounted in Prolong Gold Antifade Mountant (Life
664 Technologies, P-36930). Images were taken on Biotek Lionheart Automatic Microscope and EU
665 intensity quantification was conducted using Biotek Gen5 software. For eGFP-TOPBP1
666 fluorescence microscopy, 50,000 cells grown on coverslips in 24-well plates were treated with
667 doxycycline (1 μg/mL) for 12 hours to express eGFP-TOPBP1. MLN4924 (1 μM) and RO3306
668 (10 μM) were added to the cell culture, and the cells were incubated for another 16 hours followed
669 by IR (10 Gy) and recovery for 2 hours. Cells were fixed in 4% Paraformaldehyde for 20 minutes
670 followed by Hoechst (1:2000) staining for DNA and mounting in Prolong Gold Antifade Mountant.
671 Images were taken and quantified on Biotek Lionheart Automatic Microscope. Representative data
672 are shown for experiments repeated three of more times with consistent results.
673
674
675 **Flow cytometry and cell cycle analysis**
676 Click-iT RNA Alexa Fluor Imaging Kit was adapted to label newly synthesized RNAs in the cells
677 for flow cytometry. Abl pre-B cells grown in 24-well plate were irradiated with 10 Gray and
678 allowed to recover for different times. 2 mM EU was added to the medium and incubated for 30
679 minutes for EU incorporation. Cells were then washed with PBS, fixed in 4% paraformaldehyde
680 PBS for 15 minutes at room temperature, and permeabilized in cold 0.5% TritonX-100 PBS for 5
681 minutes. Click-iT reaction cocktail was prepared according to the manufacturer's protocol and
682 immediately added to the cells to perform click reaction in the dark for 30 minutes at room

683 temperature. Cells were then washed with Click-iT reaction rinse buffer (Component F) and 3%
684 BSA-PBS, respectively. For cell cycle analysis, BrdU (10 ug/mL) was added to the cells and
685 incubated for 30 minutes to label new DNAs. Cells were washed with PBS, fixed in 4%
686 paraformaldehyde PBS for 15 minutes at room temperature, and permeabilized in cold 0.5% Triton
687 X-100 PBS for 5 minutes. Cells were then digested with DNase (BD Biosciences, 51-2358KC) for
688 1 hour at 37 °C. Subsequently, cells were incubated with Alexa Fluor 488 Mouse anti-BrdU (BD
689 Biosciences, 51-9004981, 1:500) in 3% BSA-FBS for 1 hour at room temperature and washed 2x
690 with PBS, followed by FxCycle Violet (Thermo Scientific, R37166) or 7-AAD (BD Pharmingen,
691 559925) staining for 10 minutes. Cells were resuspended in PBS and analyzed on BD LSRII Flow
692 Cytometer or BD LSRFortessa Flow Cytometer. Flow cytometry results were further analyzed
693 using FlowJo software. Representative data are shown for experiments repeated three of more
694 times with consistent results.
695
696 **CRISPR-Cas9 screen**
697 More than 140 million wild type Abl pre-B cells carrying inducible Cas9 transgene were
698 transduced with a lentiviral gRNA library containing 90,230 gRNAs targeting over 18,000 mouse
699 genes (Addgene, 67988) by spin-infection as described above. 3 days post infection, cells
700 transduced with gRNAs were sorted on a BD FACSAria II Cell Sorter based on BFP expression.
701 BFP positive cells were treated 3 μg/ml doxycycline for 7 days to induce gRNA expression and
702 gene inactivation. Cells were irradiated with 10 Gray, allowed to recover for 30 minutes, processed
703 as described above for EU labeling of newly synthesized RNAs and analyzed on BD FACSAria II
704 Cell Sorter. Cells with high (top 10%) EU staining and unsorted cells were collected, and genomic
705 DNA of the cells were isolated for library preparation using nested-PCR. The library was

706 sequenced on an Illumina HiSeq 2500 platform. Raw fastq files were demultiplexed by the
707 Genomics and Epigenomics Core Facility of the Weill Cornell Medicine Core Laboratories Center.
708 The gRNA sequence region was then retrieved from the sequencing data using Seqkit (Shen et al.,
709 2016) and mapped to the gRNA sequence library (Koike-Yusa et al., 2014, Tzelepis et al., 2016).
710 The number of reads of each library sequence was counted and then normalized as follows (Shalem
711 et al., 2014). Normalized reads per gRNA = reads pers gRNA total reads for all sgRNAs in
712 sample$\times 10^6$+1. Hereby, the generated normalized reads from each guide RNA were used and
713 compared between the EU high cell and unsorted cell. P values were measured by Poisson test to
714 compare guide RNAs between EU high cell and unsorted cell. FDR was used for adjusting P value.
715 CRISPR score = log2 (final sgRNA abundance/initial sgRNA abundance). The EU high genes
716 were defined as these genes that have at least one guide RNA with P adjust value <=0.01 & FC
717 >=1.5. Gene ontology (GO) analysis was performed by the R package cluster Profiler v3.18.1.
718

719 **Isolation and deep sequencing of EU labeled nascent transcripts**

720 Click-iT Nascent RNA Capture Kit (Thermo Fisher, C10365) was used to label and capture the
721 nascent transcripts. In brief, the same number of Abl pre-B cells was plated in two T-25
722 Polystyrene flasks, one for irradiation (10 Gray) and the other for no IR control. After irradiation,
723 both flasks of cells were recovered for 30 minutes and incubated in medium with 2 mM EU for 30
724 minutes to allow for the incorporation of EU into the nascent transcripts. Total RNAs were
725 harvested using TRIzol reagent (Thermo Fischer, 15596018) following the manufacturer's
726 protocol. The click-iT reaction was performed as per manufacturer's protocol in 50 μL total
727 volume for 30 minutes in the dark. Subsequently, 1 μL ultrapure glycogen, 50 μL 7.5 M
728 ammonium acetate, and 700 μL of chilled 100% EtOH were added to the reaction. The mixture

729 was incubated at −80 °C for 16 hours. RNA pellet was spun down at 13000 ×g for 20 minutes at
730 4 °C, washed 2x with chilled 75% EtOH and resuspended in nuclease free water. EU-RNAs were
731 pulled down with Dynabeads MyOne Streptavidin T1 magnetic beads and extracted with TRIzol
732 reagents. The same amount of ERCC spike-ins (Thermo Fisher, 4456740) were added to the
733 purified EU-RNAs, followed by cDNA library generation using NEBNext Ultr II Directional RNA
734 Library Prep Kit for Illumina (NEB, E7760) according to the manufacturer's protocol and deep
735 sequencing on Illumina HiSeq 2500 platform.
736
737 **Real-time quantitative RT-PCR of EU labeled nascent transcripts**
738 EU labeled RNA was prepared from the same number of cells as described above. All the isolated
739 EU-RNAs were used for cDNA synthesis using Superscript III (Thermo Fischer, 18080044)
740 reverse transcription with random hexamer as primers following the manufacturer's protocol. The
741 same proportion of cDNA products of each sample was used as template for the quantitative RT-
742 PCR reaction with Light Cycler 480 SYBR Green I Master Mix (Roche, 04707516001). The Ct
743 value was used to represent the absolute amount of EU-RNAs in each sample, in which a smaller
744 Ct value indicates higher nascent transcript levels of an individual gene, given the same initial
745 number of cells and the same proportion of EU-RNAs were used for the analyses. Primer
746 sequences for the analyses are as follows:
747 ms28S-fwd, 5'-TGGGTTTTAAGCAGGAGGTG-; ms28S-rev, 5'-
748 GTGAATTCTGCTTCACAATG-3'(Watada et al., 2020); ms18S-fwd, 5'-
749 CTTAGAGGGACAAGTGGCG-3'; ms18S-rev, 5'-ACGCTGAGCCAGTCAGTGTA-3'
750 (Stephens et al., 2011); msHist1h2ab-fwd, 5'-GCCTGCAGTTCCCCGTA-3'; msHisth2ab-rev,
751 5'- ATCTCGGCCGTCAGGTACTC-3'; msHist1h2ac-fwd, 5'-GGCTGCTCCGCAAGGGT-3';

752 msHist1h2ac-rev, 5'-CTTGTTGAGCTCCTCGTCGTT-3'; msH2afz-fwd, 5'-
753 ACTCCGGAAAGGCCAAGACA-3'; msH2afz-rev, 5'-GTTGTCCTAGATTTCAGGTG-3'
754 (Nishida et al., 2005); msCdkn1a-fwd, 5'-GTGGCCTTGTCGCTGTCT-3'; msCdkn1a-rev, 5'-
755 TTTTCTCTTGCAGAAGACCAATC-3' (Béguelin et al., 2017).
756

757 **Analysis of nascent transcripts**

758 The mouse genome version GRCm38.p6 release M23 and the associated GENCODE version of
759 mouse reference gene set were downloaded from the GENCODE website
760 (https://www.gencodegenes.org/mouse/release_M23.html). We trimmed adapter sequences and
761 low-quality sequences in RNA-seq data using the Trim Galore v0.6.6 (Martin, 2011) with default
762 parameters. To avoid rRNA homologous sequences (i.e., in the intron regions of Zc3h7a or Cdk8)
763 prior to subsequent genomic and other RNA analysis, we first mapped the reads to mm10 rDNA
764 sequences by TopHat v2.1.1 (Kim et al., 2013). The unmapped reads were then further mapped to
765 the mouse genome version mm10 and ERCC spike-in version ERCC92 using TopHat v2.1.1 (Kim
766 et al., 2013). Successfully mapping reads were sorted by SAMtools v1. 5. Afterward, read counts
767 in several types of genomic feature, i.e., protein-coding genes, rDNA and ERCCs (ERCC92.gtf),
768 were quantified by Htseq-count v0.11.2 (Anders et al., 2015) using the union gene region option.
769 The read number per gene was normalized based on total ERCC read numbers in each sample.
770 To visualize read coverage across the genome, DeepTools v3.5.0 (Ramírez et al., 2014) was used
771 to convert BAM files into bigwig files using scale factors calculated by total ERCC read number
772 in each sample. Next, DeepTools was used to plot average read depth per sample across interested
773 groups of genomic regions (i.e., repressed protein coding genes from 3 kb upstream to 3kb

774 downstream of gene bodies). Screenshots of reads density at individual regions were generated by
775 IGV 2.8.13 (Thorvaldsdóttir et al., 2013).
776 We then used one tail Poisson test to evaluate difference in gene expression level based on the read
777 counts normalized by total ERCC read counts. We defined differentially expressed RNAs as those
778 with a fold change greater than 1.5 and an FDR value smaller than 0.05. To detect highly expressed
779 genes, we ranked genes by RPKM in the control cells, whereas RPKM was calculated using
780 ERCC-normalized read counts further normalized by gene length. Gene ontology (GO) analysis
781 was performed by the R package clusterProfiler v3.18.1 (Wu et al., 2021). Heatmap were generated
782 by pheatmap.
783
784 **Data availability**
785 All raw datasets of nascent EU RNA-seq and CRISPR screen data have been submitted to GEO
786 (GSE217123) and available by Project: PRJNA895065.
787
788 **Acknowledgements**
789 The authors thank Yinan Wang for performing the bioinformatics for the high throughput screen.
790 We thank the Weill Cornell Flow Cytometry Core for flow cytometry. We thank the Weill Cornell
791 Epigenomics Core for performing the sequencing for the high throughput screen and the
792 Transcriptional Regulation & Expression Facility at Cornell University, Ithaca for providing
793 advice and performing the sequencing of the nascent transcripts. The stable doxycycline-inducible
794 eGFP-TOPBP1 U2OS cell lines were a kind gift from Dr. Helmut Pospiech (Fritz Lipmann
795 Institute, Germany). We are grateful to Pengbo Zhou for advice on Cullin 4A and B. We also thank
796 Barry Sleckman, Bo-Ruei Chen and Faith Fowler for advice throughout the project. JKT is

797 supported by NIH R35 GM139816 and RO1 CA95641. K.C is supported by NIH R01GM138407,
798 R01GM125632, R01HL148338, and R01HL133254.

799

800 **References**

801 ADAM, S., POLO, S. E. & ALMOUZNI, G. 2013. Transcription recovery after DNA damage requires
802 chromatin priming by the H3.3 histone chaperone HIRA. *Cell,* 155**,** 94-106.
803 ANDERS, S., PYL, P. T. & HUBER, W. 2015. HTSeq—a Python framework to work with high-
804 throughput sequencing data. *bioinformatics,* 31**,** 166-169.
805 ARTUSO, M., ESTEVE, A., BRESIL, H., VUILLAUME, M. & HALL, J. 1995. The role of the Ataxia
806 telangiectasia gene in the p53, WAF1/CIP1(p21)- and GADD45-mediated response to
807 DNA damage produced by ionising radiation. *Oncogene,* 11**,** 1427-35.
808 BÉGUELIN, W., RIVAS, M. A., CALVO FERNÁNDEZ, M. T., TEATER, M., PURWADA, A., REDMOND,
809 D., SHEN, H., CHALLMAN, M. F., ELEMENTO, O., SINGH, A. & MELNICK, A. M. 2017. EZH2
810 enables germinal centre formation through epigenetic silencing of CDKN1A and an Rb-
811 E2F1 feedback loop. *Nat Commun,* 8**,** 877.
812 BLACKFORD, A. N. & JACKSON, S. P. 2017. ATM, ATR, and DNA-PK: The Trinity at the Heart of
813 the DNA Damage Response. *Mol Cell,* 66**,** 801-817.
814 BOUVIER, D., FERRAND, J., CHEVALLIER, O., PAULSEN, M. T., LJUNGMAN, M. & POLO, S. E. 2021.
815 Dissecting regulatory pathways for transcription recovery following DNA damage reveals
816 a non-canonical function of the histone chaperone HIRA. *Nat Commun,* 12**,** 3835.
817 BREDEMEYER, A. L., SHARMA, G. G., HUANG, C. Y., HELMINK, B. A., WALKER, L. M., KHOR, K. C.,
818 NUSKEY, B., SULLIVAN, K. E., PANDITA, T. K., BASSING, C. H. & SLECKMAN, B. P. 2006.
819 ATM stabilizes DNA double-strand-break complexes during V(D)J recombination. *Nature,*
820 442**,** 466-70.
821 BROWN, J. S., LUKASHCHUK, N., SCZANIECKA-CLIFT, M., BRITTON, S., LE SAGE, C., CALSOU, P.,
822 BELI, P., GALANTY, Y. & JACKSON, S. P. 2015. Neddylation promotes ubiquitylation and
823 release of Ku from DNA-damage sites. *Cell Rep,* 11**,** 704-14.
824 CARON, P., PANKOTAI, T., WIEGANT, W. W., TOLLENAERE, M. A. X., FURST, A., BONHOMME, C.,
825 HELFRICHT, A., DE GROOT, A., PASTINK, A., VERTEGAAL, A. C. O., LUIJSTERBURG, M. S.,
826 SOUTOGLOU, E. & VAN ATTIKUM, H. 2019. WWP2 ubiquitylates RNA polymerase II for
827 DNA-PK-dependent transcription arrest and repair at DNA breaks. *Genes Dev,* 33**,** 684-
828 704.
829 CHEN, B. R., WANG, Y., TUBBS, A., ZONG, D., FOWLER, F. C., ZOLNEROWICH, N., WU, W.,
830 BENNETT, A., CHEN, C. C., FENG, W., NUSSENZWEIG, A., TYLER, J. K. & SLECKMAN, B. P.
831 2021. LIN37-DREAM prevents DNA end resection and homologous recombination at
832 DNA double-strand breaks in quiescent cells. *Elife,* 10.
833 HANNAH, J. & ZHOU, P. 2015. Distinct and overlapping functions of the cullin E3 ligase
834 scaffolding proteins CUL4A and CUL4B. *Gene,* 573**,** 33-45.
835 HUANG, T. H., FOWLER, F., CHEN, C. C., SHEN, Z. J., SLECKMAN, B. & TYLER, J. K. 2018. The
836 Histone Chaperones ASF1 and CAF-1 Promote MMS22L-TONSL-Mediated Rad51 Loading

837 onto ssDNA during Homologous Recombination in Human Cells. *Mol Cell,* 69**,** 879-892
838 e5.
839 IANNELLI, F., GALBIATI, A., CAPOZZO, I., NGUYEN, Q., MAGNUSON, B., MICHELINI, F.,
840 D'ALESSANDRO, G., CABRINI, M., RONCADOR, M., FRANCIA, S., CROSETTO, N.,
841 LJUNGMAN, M., CARNINCI, P. & D'ADDA DI FAGAGNA, F. 2017. A damaged genome's
842 transcriptional landscape through multilayered expression profiling around in situ-
843 mapped DNA double-strand breaks. *Nat Commun,* 8**,** 15656.
844 JACKSON, S. P. & BARTEK, J. 2009. The DNA-damage response in human biology and disease.
845 *Nature,* 461**,** 1071-8.
846 JAO, C. Y. & SALIC, A. 2008. Exploring RNA transcription and turnover in vivo by using click
847 chemistry. *Proc Natl Acad Sci U S A,* 105**,** 15779-84.
848 KAKAROUGKAS, A., ISMAIL, A., CHAMBERS, A. L., RIBALLO, E., HERBERT, A. D., KUNZEL, J.,
849 LOBRICH, M., JEGGO, P. A. & DOWNS, J. A. 2014. Requirement for PBAF in
850 transcriptional repression and repair at DNA breaks in actively transcribed regions of
851 chromatin. *Mol Cell,* 55**,** 723-32.
852 KIM, D., PERTEA, G., TRAPNELL, C., PIMENTEL, H., KELLEY, R. & SALZBERG, S. L. 2013. TopHat2:
853 accurate alignment of transcriptomes in the presence of insertions, deletions and gene
854 fusions. *Genome biology,* 14**,** 1-13.
855 KOIKE-YUSA, H., LI, Y., TAN, E. P., VELASCO-HERRERA, M. E. C. & YUSA, K. 2014. Genome-wide
856 recessive genetic screening in mammalian cells with a lentiviral CRISPR-guide RNA
857 library. *Nat Biotechnol,* 32**,** 267-73.
858 KRUHLAK, M., CROUCH, E. E., ORLOV, M., MONTANO, C., GORSKI, S. A., NUSSENZWEIG, A.,
859 MISTELI, T., PHAIR, R. D. & CASELLAS, R. 2007. The ATM repair pathway inhibits RNA
860 polymerase I transcription in response to chromosome breaks. *Nature,* 447**,** 730-4.
861 LARSEN, D. H., HARI, F., CLAPPERTON, J. A., GWERDER, M., GUTSCHE, K., ALTMEYER, M.,
862 JUNGMICHEL, S., TOLEDO, L. I., FINK, D., RASK, M. B., GRØFTE, M., LUKAS, C., NIELSEN,
863 M. L., SMERDON, S. J., LUKAS, J. & STUCKI, M. 2014. The NBS1-Treacle complex controls
864 ribosomal RNA transcription in response to DNA damage. *Nat Cell Biol,* 16**,** 792-803.
865 LIEBERMAN, H. B., PANIGRAHI, S. K., HOPKINS, K. M., WANG, L. & BROUSTAS, C. G. 2017. p53
866 and RAD9, the DNA Damage Response, and Regulation of Transcription Networks.
867 *Radiat Res,* 187**,** 424-432.
868 MA, T., VAN TINE, B. A., WEI, Y., GARRETT, M. D., NELSON, D., ADAMS, P. D., WANG, J., QIN, J.,
869 CHOW, L. T. & HARPER, J. W. 2000. Cell cycle-regulated phosphorylation of p220(NPAT)
870 by cyclin E/Cdk2 in Cajal bodies promotes histone gene transcription. *Genes Dev,* 14**,**
871 2298-313.
872 MARTIN, M. 2011. Cutadapt removes adapter sequences from high-throughput sequencing
873 reads. *EMBnet. journal,* 17**,** 10-12.
874 MEISENBERG, C., PINDER, S. I., HOPKINS, S. R., WOOLLER, S. K., BENSTEAD-HUME, G., PEARL, F.
875 M. G., JEGGO, P. A. & DOWNS, J. A. 2019. Repression of Transcription at DNA Breaks
876 Requires Cohesin throughout Interphase and Prevents Genome Instability. *Mol Cell,* 73**,**
877 212-223 e7.
878 MOOSER, C., SYMEONIDOU, I. E., LEIMBACHER, P. A., RIBEIRO, A., SHORROCKS, A. K.,
879 JUNGMICHEL, S., LARSEN, S. C., KNECHTLE, K., JASROTIA, A., ZURBRIGGEN, D.,
880 JEANRENAUD, A., LEIKAUF, C., FINK, D., NIELSEN, M. L., BLACKFORD, A. N. & STUCKI, M.

881 2020. Treacle controls the nucleolar response to rDNA breaks via TOPBP1 recruitment
882 and ATR activation. *Nat Commun,* 11**,** 123.
883 MOSS, T. & STEFANOVSKY, V. Y. 1995. Promotion and regulation of ribosomal transcription in
884 eukaryotes by RNA polymerase I. *Prog Nucleic Acid Res Mol Biol,* 50**,** 25-66.
885 NISHIDA, H., SUZUKI, T., OOKAWA, H., TOMARU, Y. & HAYASHIZAKI, Y. 2005. Comparative
886 analysis of expression of histone H2a genes in mouse. *BMC Genomics,* 6**,** 108.
887 O'MAHONY, D. J., XIE, W. Q., SMITH, S. D., SINGER, H. A. & ROTHBLUM, L. I. 1992. Differential
888 phosphorylation and localization of the transcription factor UBF in vivo in response to
889 serum deprivation. In vitro dephosphorylation of UBF reduces its transactivation
890 properties. *J Biol Chem,* 267**,** 35-8.
891 PAN, Z. Q., KENTSIS, A., DIAS, D. C., YAMOAH, K. & WU, K. 2004. Nedd8 on cullin: building an
892 expressway to protein destruction. *Oncogene,* 23**,** 1985-97.
893 PANKOTAI, T., BONHOMME, C., CHEN, D. & SOUTOGLOU, E. 2012. DNAPKcs-dependent arrest
894 of RNA polymerase II transcription in the presence of DNA breaks. *Nat Struct Mol Biol,*
895 19**,** 276-82.
896 PANKOTAI, T. & SOUTOGLOU, E. 2013. Double strand breaks: hurdles for RNA polymerase II
897 transcription? *Transcription,* 4**,** 34-8.
898 PORTER, J. R., FISHER, B. E., BARANELLO, L., LIU, J. C., KAMBACH, D. M., NIE, Z., KOH, W. S., LUO,
899 J., STOMMEL, J. M., LEVENS, D. & BATCHELOR, E. 2017. Global Inhibition with Specific
900 Activation: How p53 and MYC Redistribute the Transcriptome in the DNA Double-Strand
901 Break Response. *Mol Cell,* 67**,** 1013-1025 e9.
902 PURMAN, C. E., COLLINS, P. L., PORTER, S. I., SAINI, A., GUPTA, H., SLECKMAN, B. P. & OLTZ, E.
903 M. 2019. Regional Gene Repression by DNA Double-Strand Breaks in G1 Phase Cells. *Mol*
904 *Cell Biol,* 39.
905 RABUT, G. & PETER, M. 2008. Function and regulation of protein neddylation. 'Protein
906 modifications: beyond the usual suspects' review series. *EMBO Rep,* 9**,** 969-76.
907 RAMÍREZ, F., DÜNDAR, F., DIEHL, S., GRÜNING, B. A. & MANKE, T. 2014. deepTools: a flexible
908 platform for exploring deep-sequencing data. *Nucleic acids research,* 42**,** W187-W191.
909 SHALEM, O., SANJANA, N. E., HARTENIAN, E., SHI, X., SCOTT, D. A., MIKKELSON, T., HECKL, D.,
910 EBERT, B. L., ROOT, D. E., DOENCH, J. G. & ZHANG, F. 2014. Genome-scale CRISPR-Cas9
911 knockout screening in human cells. *Science,* 343**,** 84-87.
912 SHANBHAG, N. M., RAFALSKA-METCALF, I. U., BALANE-BOLIVAR, C., JANICKI, S. M. &
913 GREENBERG, R. A. 2010. ATM-dependent chromatin changes silence transcription in cis
914 to DNA double-strand breaks. *Cell,* 141**,** 970-81.
915 SHEN, W., LE, S., LI, Y. & HU, F. 2016. SeqKit: A Cross-Platform and Ultrafast Toolkit for FASTA/Q
916 File Manipulation. *PLoS One,* 11**,** e0163962.
917 SITTMAN, D. B., GRAVES, R. A. & MARZLUFF, W. F. 1983. Histone mRNA concentrations are
918 regulated at the level of transcription and mRNA degradation. *Proc Natl Acad Sci U S A,*
919 80**,** 1849-53.
920 SOKKA, M., RILLA, K., MIINALAINEN, I., POSPIECH, H. & SYVÄOJA, J. E. 2015. High levels of
921 TopBP1 induce ATR-dependent shut-down of rRNA transcription and nucleolar
922 segregation. *Nucleic Acids Res,* 43**,** 4975-89.

923 STEPHENS, A. S., STEPHENS, S. R. & MORRISON, N. A. 2011. Internal control genes for
924 quantitative RT-PCR expression analysis in mouse osteoblasts, osteoclasts and
925 macrophages. *BMC Res Notes,* 4**,** 410.
926 SU, C., GAO, G., SCHNEIDER, S., HELT, C., WEISS, C., O'REILLY, M. A., BOHMANN, D. & ZHAO, J.
927 2004. DNA damage induces downregulation of histone gene expression through the G1
928 checkpoint pathway. *EMBO J,* 23**,** 1133-43.
929 THORVALDSDÓTTIR, H., ROBINSON, J. T. & MESIROV, J. P. 2013. Integrative Genomics Viewer
930 (IGV): high-performance genomics data visualization and exploration. *Briefings in*
931 *bioinformatics,* 14**,** 178-192.
932 TZELEPIS, K., KOIKE-YUSA, H., DE BRAEKELEER, E., LI, Y., METZAKOPIAN, E., DOVEY, O. M.,
933 MUPO, A., GRINKEVICH, V., LI, M., MAZAN, M., GOZDECKA, M., OHNISHI, S., COOPER, J.,
934 PATEL, M., MCKERRELL, T., CHEN, B., DOMINGUES, A. F., GALLIPOLI, P., TEICHMANN, S.,
935 PONSTINGL, H., MCDERMOTT, U., SAEZ-RODRIGUEZ, J., HUNTLY, B. J. P., IORIO, F., PINA,
936 C., VASSILIOU, G. S. & YUSA, K. 2016. A CRISPR Dropout Screen Identifies Genetic
937 Vulnerabilities and Therapeutic Targets in Acute Myeloid Leukemia. *Cell Rep,* 17**,** 1193-
938 1205.
939 VAN SLUIS, M. & MCSTAY, B. 2017. Nucleolar reorganization in response to rDNA damage. *Curr*
940 *Opin Cell Biol,* 46**,** 81-86.
941 VASSILEV, L. T., TOVAR, C., CHEN, S., KNEZEVIC, D., ZHAO, X., SUN, H., HEIMBROOK, D. C. &
942 CHEN, L. 2006. Selective small-molecule inhibitor reveals critical mitotic functions of
943 human CDK1. *Proc Natl Acad Sci U S A,* 103**,** 10660-5.
944 VENKATA NARAYANAN, I., PAULSEN, M. T., BEDI, K., BERG, N., LJUNGMAN, E. A., FRANCIA, S.,
945 VELOSO, A., MAGNUSON, B., DI FAGAGNA, F. D., WILSON, T. E. & LJUNGMAN, M. 2017.
946 Transcriptional and post-transcriptional regulation of the ionizing radiation response by
947 ATM and p53. *Sci Rep,* 7**,** 43598.
948 WATADA, E., LI, S., HORI, Y., FUJIKI, K., SHIRAHIGE, K., INADA, T. & KOBAYASHI, T. 2020. Age-
949 Dependent Ribosomal DNA Variations in Mice. *Mol Cell Biol,* 40.
950 WU, T., HU, E., XU, S., CHEN, M., GUO, P., DAI, Z., FENG, T., ZHOU, L., TANG, W. & ZHAN, L.
951 2021. clusterProfiler 4.0: A universal enrichment tool for interpreting omics data. *The*
952 *Innovation,* 2**,** 100141.
953 ZHAO, J., DYNLACHT, B., IMAI, T., HORI, T. & HARLOW, E. 1998. Expression of NPAT, a novel
954 substrate of cyclin E-CDK2, promotes S-phase entry. *Genes Dev,* 12**,** 456-61.
955 ZHAO, J., KENNEDY, B. K., LAWRENCE, B. D., BARBIE, D. A., MATERA, A. G., FLETCHER, J. A. &
956 HARLOW, E. 2000. NPAT links cyclin E-Cdk2 to the regulation of replication-dependent
957 histone gene transcription. *Genes Dev,* 14**,** 2283-97.
958

**Figure 1**

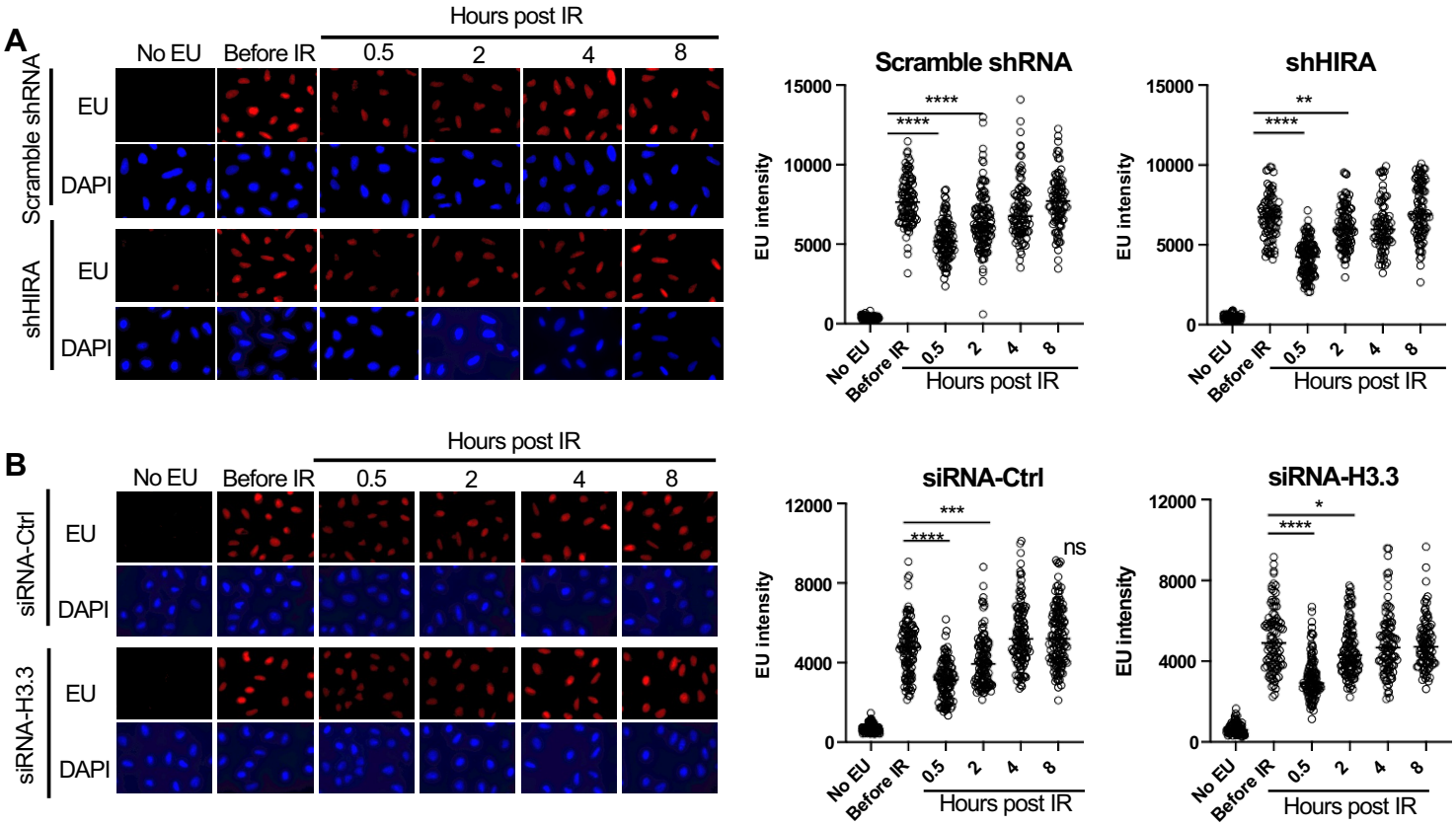
A
Hours post IR
No EU
Before IR
0.5
2
4
8
Scramble shRNA
shHIRA
EU
DAPI
Scramble shRNA
shHIRA
EU intensity
15000
10000
5000
0
****
**
Hours post IR
B
siRNA-Ctrl
siRNA-H3.3
12000
8000
4000
***
*
ns

**Figure 2**

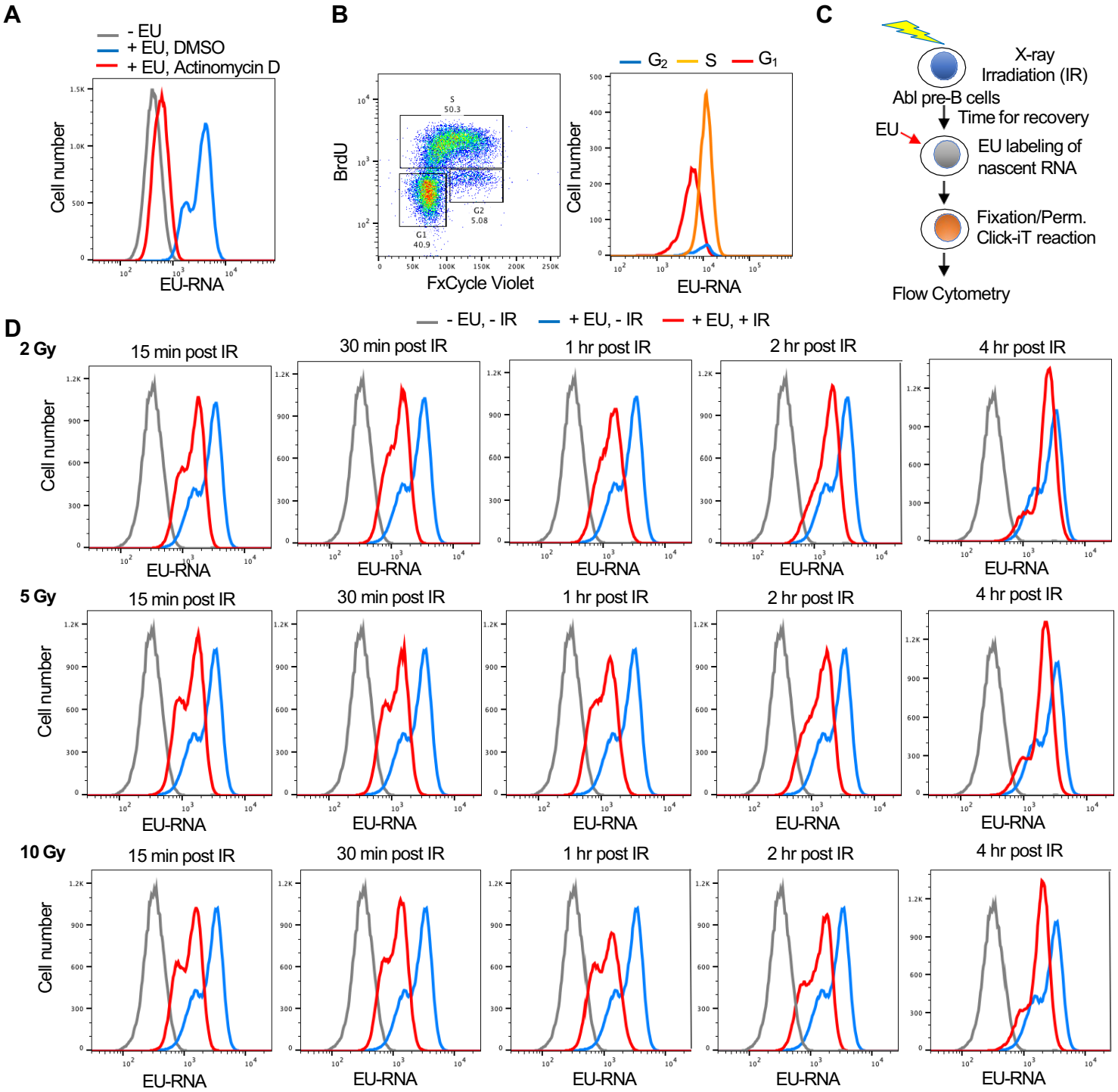
A
- EU
+ EU, DMSO
+ EU, Actinomycin D
Cell number
EU-RNA
B
S
50.3
G2
5.08
G1
40.9
BrdU
FxCycle Violet
G2
S
G1
Cell number
EU-RNA
C
X-ray
Irradiation (IR)
Abl pre-B cells
Time for recovery
EU
EU labeling of
nascent RNA
Fixation/Perm.
Click-iT reaction
Flow Cytometry
D
- EU, - IR
+ EU, - IR
+ EU, + IR
2 Gy
5 Gy
10 Gy
15 min post IR
30 min post IR
1 hr post IR
2 hr post IR
4 hr post IR
Cell number
EU-RNA

**Figure 3**

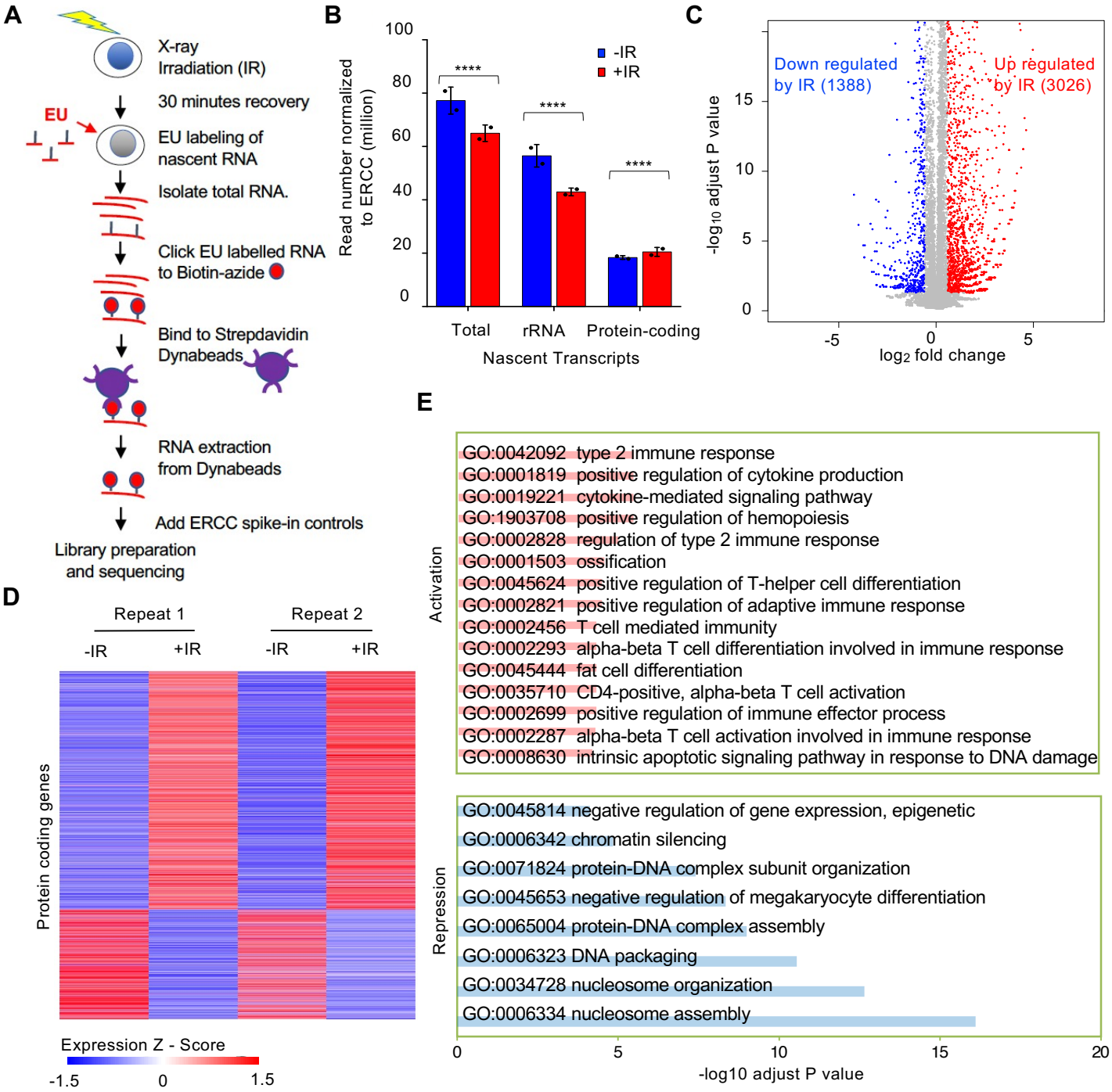
A
X-ray
Irradiation (IR)
30 minutes recovery
EU
EU labeling of
nascent RNA
Isolate total RNA.
Click EU labelled RNA
to Biotin-azide
Bind to Strepdavidin
Dynabeads
RNA extraction
from Dynabeads
Add ERCC spike-in controls
Library preparation
and sequencing
B
Read number normalized
to ERCC (million)
-IR
+IR
****
Total
rRNA
Protein-coding
Nascent Transcripts
C
Down regulated
by IR (1388)
Up regulated
by IR (3026)
-log10 adjust P value
log2 fold change
D
Repeat 1
Repeat 2
-IR
+IR
Protein coding genes
Expression Z - Score
-1.5
0
1.5
E
Activation
GO:0042092 type 2 immune response
GO:0001819 positive regulation of cytokine production
GO:0019221 cytokine-mediated signaling pathway
GO:1903708 positive regulation of hemopoiesis
GO:0002828 regulation of type 2 immune response
GO:0001503 ossification
GO:0045624 positive regulation of T-helper cell differentiation
GO:0002821 positive regulation of adaptive immune response
GO:0002456 T cell mediated immunity
GO:0002293 alpha-beta T cell differentiation involved in immune response
GO:0045444 fat cell differentiation
GO:0035710 CD4-positive, alpha-beta T cell activation
GO:0002699 positive regulation of immune effector process
GO:0002287 alpha-beta T cell activation involved in immune response
GO:0008630 intrinsic apoptotic signaling pathway in response to DNA damage
Repression
GO:0045814 negative regulation of gene expression, epigenetic
GO:0006342 chromatin silencing
GO:0071824 protein-DNA complex subunit organization
GO:0045653 negative regulation of megakaryocyte differentiation
GO:0065004 protein-DNA complex assembly
GO:0006323 DNA packaging
GO:0034728 nucleosome organization
GO:0006334 nucleosome assembly
-log10 adjust P value

## Figure 4

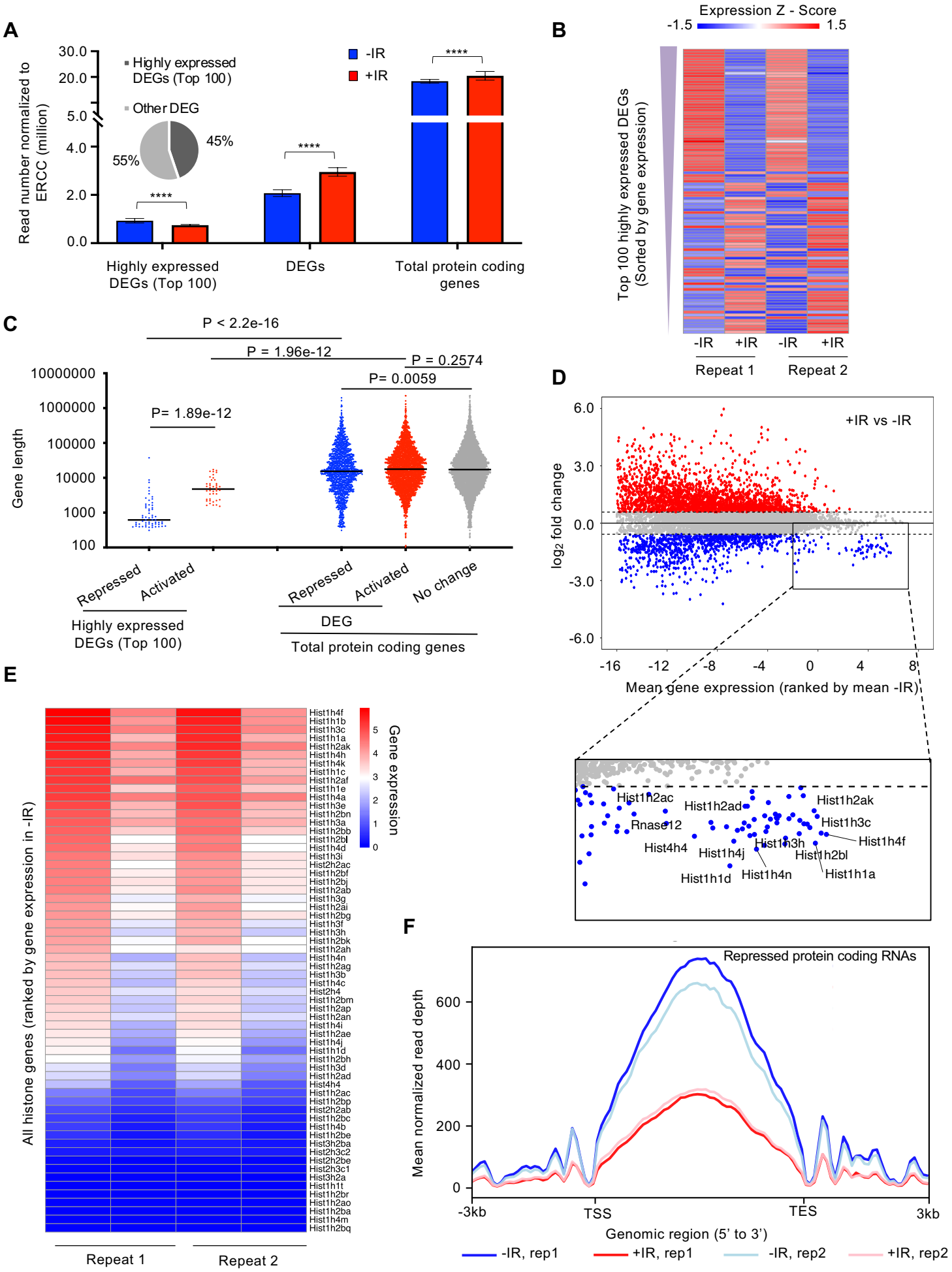
A
Read number normalized to ERCC (million)
Highly expressed DEGs (Top 100)
Other DEG
55%
45%
-IR
+IR
****
Highly expressed DEGs (Top 100)
DEGs
Total protein coding genes
B
Expression Z - Score
-1.5
1.5
Top 100 highly expressed DEGs (Sorted by gene expression)
-IR
+IR
Repeat 1
Repeat 2
C
P < 2.2e-16
P = 1.96e-12
P = 0.2574
P= 0.0059
P= 1.89e-12
Gene length
Repressed
Activated
No change
Highly expressed DEGs (Top 100)
DEG
Total protein coding genes
D
+IR vs -IR
log2 fold change
Mean gene expression (ranked by mean -IR)
Hist1h2ac
Hist1h2ad
Hist1h2ak
Rnase12
Hist1h3c
Hist4h4
Hist1h4j
Hist1h3h
Hist1h4f
Hist1h2bl
Hist1h1d
Hist1h4n
Hist1h1a
E
All histone genes (ranked by gene expression in -IR)
Gene expression
Repeat 1
Repeat 2
F
Repressed protein coding RNAs
Mean normalized read depth
-3kb
TSS
TES
3kb
Genomic region (5' to 3')
-IR, rep1
+IR, rep1
-IR, rep2
+IR, rep2

**Figure 5**

**A**

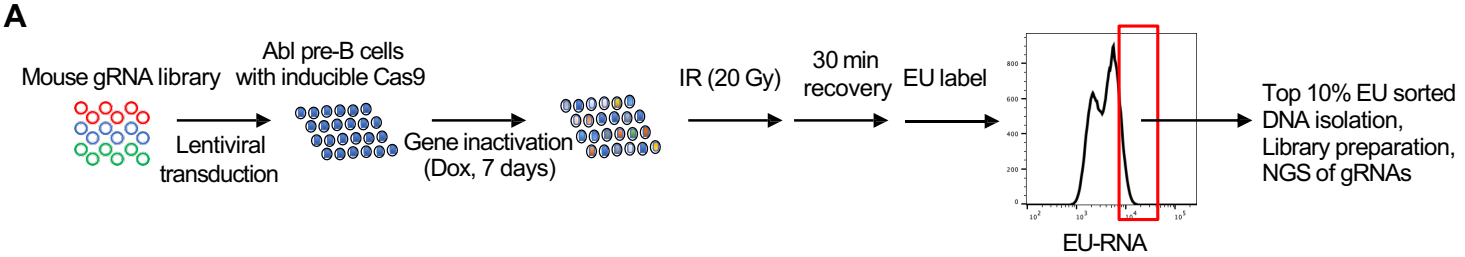


**B**

| Gene | Score | Gene | Score | Gene | Score |
|---|---|---|---|---|---|
| *Atm* | 4.7 | *Uba3* | 1.6 | *Rbx1* | 3.3 |
| | 3.1 | | 2.8 | | 2.8 |
| | 2.7 | | 3.4 | | 0.9 |
| | 1.8 | | 3.8 | | 4.1 |
| | 1.6 | | 4.1 | | 6.0 |
| *Nedd8* | 1.4 | *Ube2m/ Ubc12* | 1.7 | *Rnf7/ Rbx2* | 0.9 |
| | 2.3 | | 2.5 | | 1.6 |
| | - | | 2.6 | | 2.1 |
| | - | | 2.7 | | 1.4 |
| | - | | - | | - |
| *Nae1* | 1.8 | *Ube2f* | 1.5 | *Cul4b* | 2.6 |
| | 2.4 | | 1.6 | | 1.2 |
| | 3.6 | | 1.2 | | 1.5 |
| | 3.8 | | 1.3 | | 2.1 |
| | 4.1 | | 0.5 | | 1.6 |

**C**

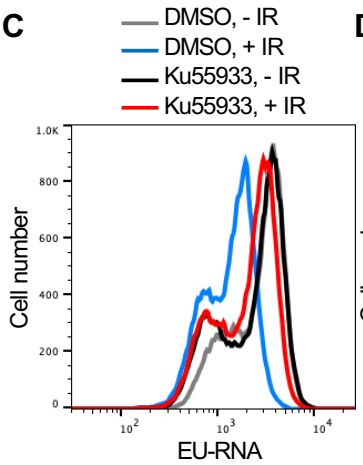


**D**

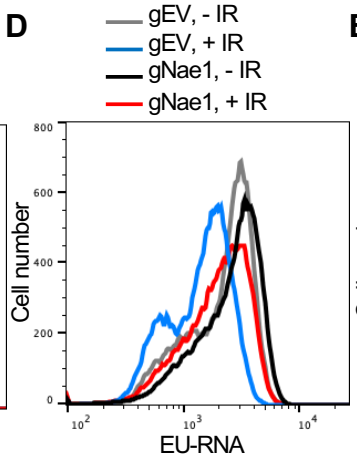


**E**

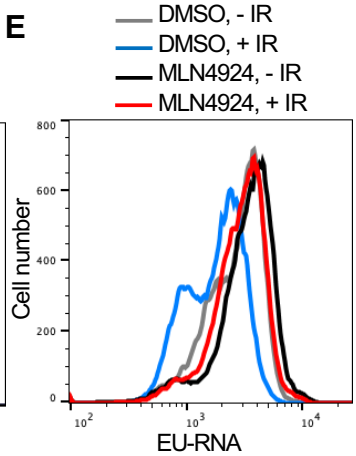


**F**

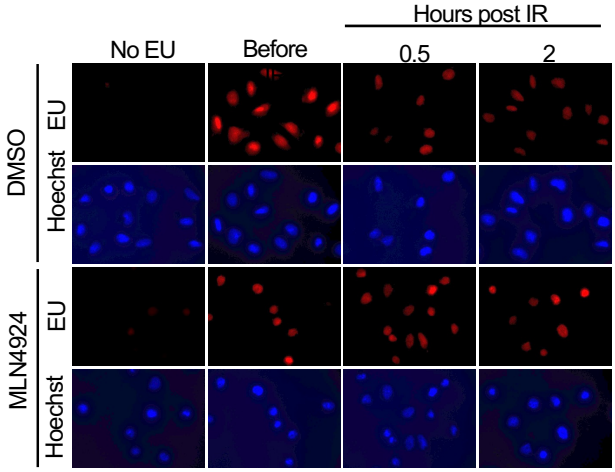


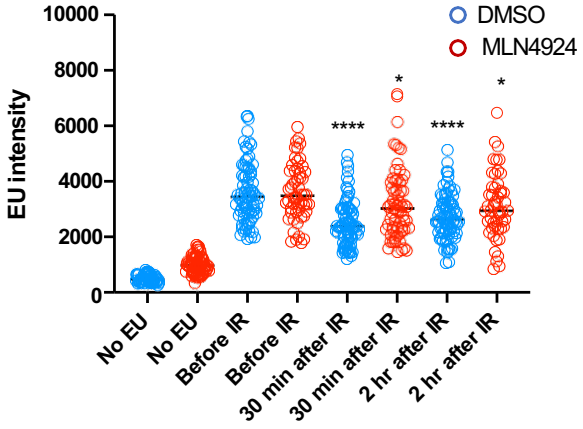

**Figure 6**

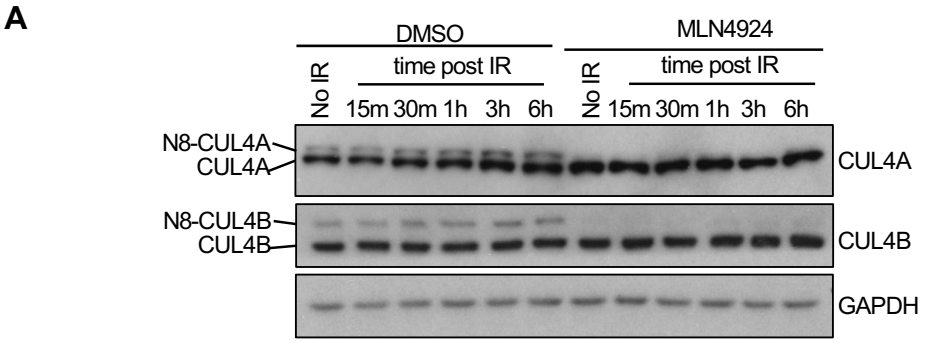
A
DMSO
MLN4924
time post IR
No IR
15m 30m 1h 3h 6h
N8-CUL4A
CUL4A
N8-CUL4B
CUL4B
CUL4A
CUL4B
GAPDH

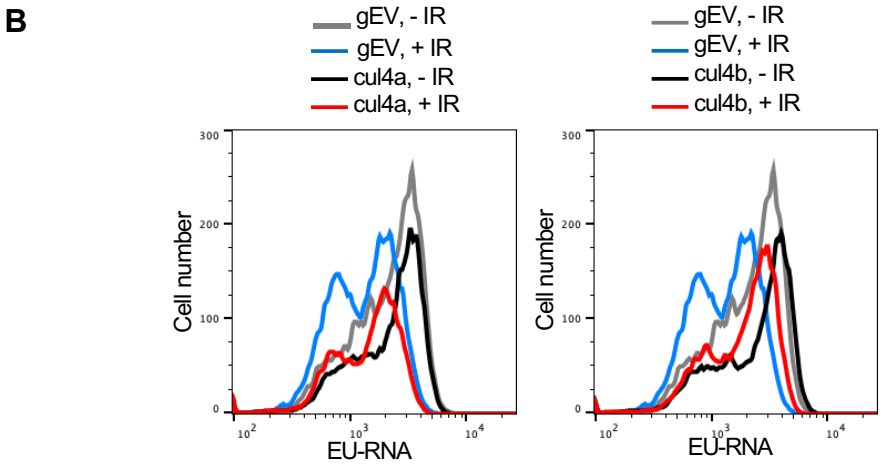
B
gEV, - IR
gEV, + IR
cul4a, - IR
cul4a, + IR
gEV, - IR
gEV, + IR
cul4b, - IR
cul4b, + IR
Cell number
EU-RNA

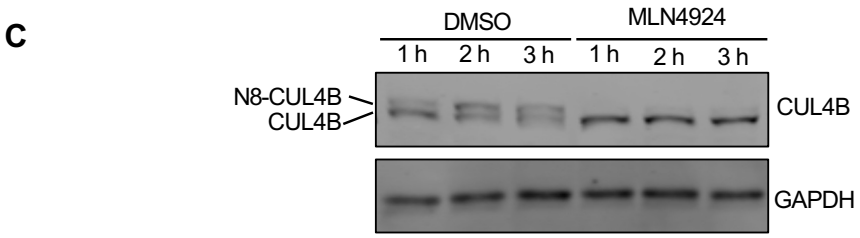
C
DMSO
MLN4924
1 h 2 h 3 h
N8-CUL4B
CUL4B
CUL4B
GAPDH

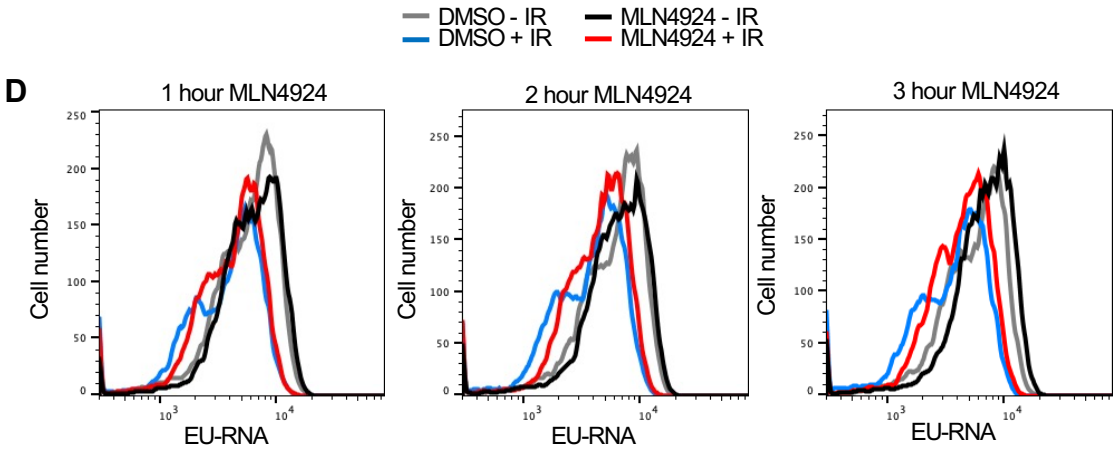
DMSO - IR
DMSO + IR
MLN4924 - IR
MLN4924 + IR
D
1 hour MLN4924
2 hour MLN4924
3 hour MLN4924
Cell number
EU-RNA

**Figure 7**

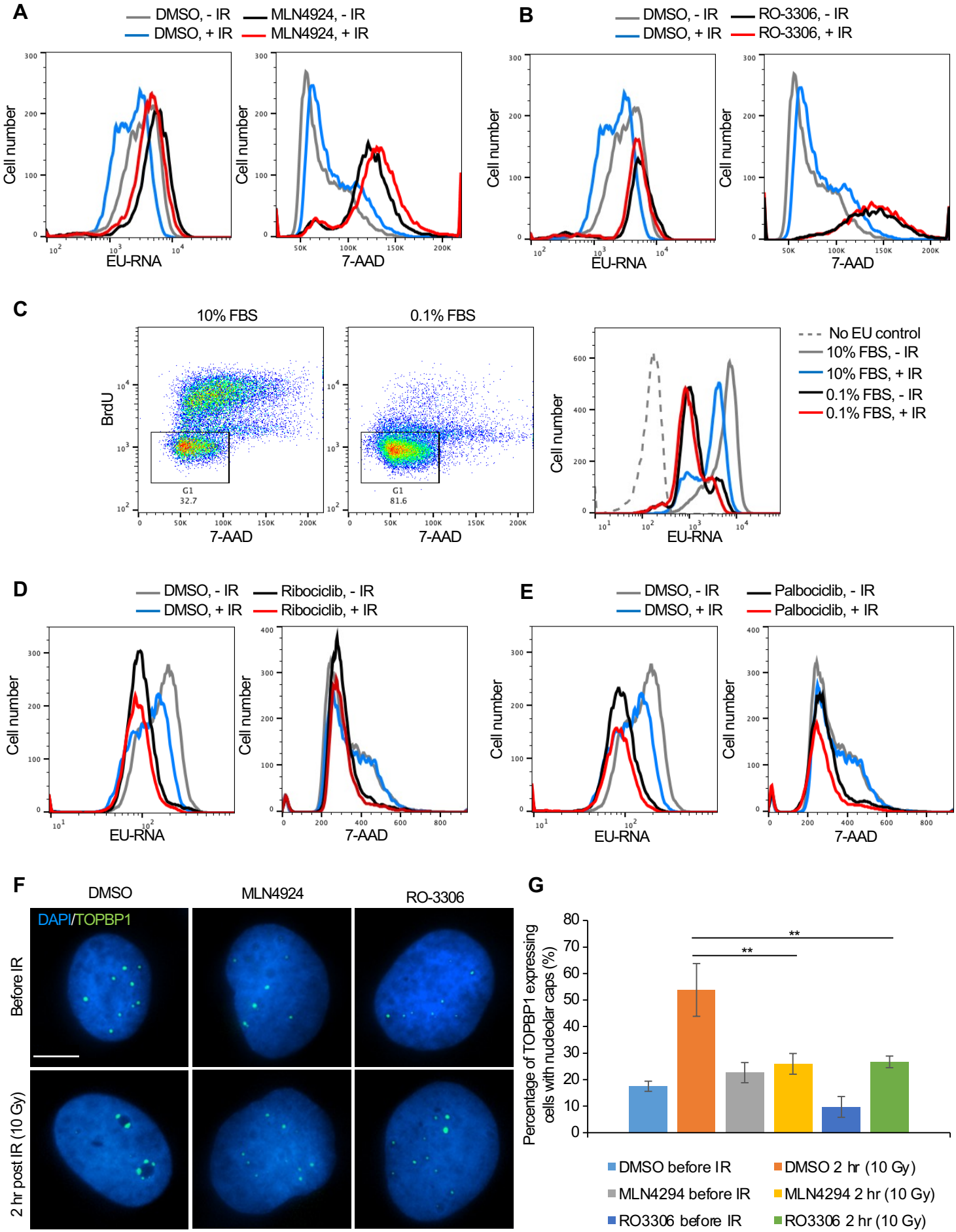
A
DMSO, - IR
DMSO, + IR
MLN4924, - IR
MLN4924, + IR
Cell number
EU-RNA
7-AAD
B
DMSO, - IR
DMSO, + IR
RO-3306, - IR
RO-3306, + IR
C
10% FBS
0.1% FBS
BrdU
G1
32.7
G1
81.6
No EU control
10% FBS, - IR
10% FBS, + IR
0.1% FBS, - IR
0.1% FBS, + IR
D
DMSO, - IR
DMSO, + IR
Ribociclib, - IR
Ribociclib, + IR
E
DMSO, - IR
DMSO, + IR
Palbociclib, - IR
Palbociclib, + IR
F
DMSO
MLN4924
RO-3306
DAPI/TOPBP1
Before IR
2 hr post IR (10 Gy)
G
Percentage of TOPBP1 expressing cells with nucleolar caps (%)
**
**
DMSO before IR
DMSO 2 hr (10 Gy)
MLN4294 before IR
MLN4294 2 hr (10 Gy)
RO3306 before IR
RO3306 2 hr (10 Gy)

**Supp Fig. 1**

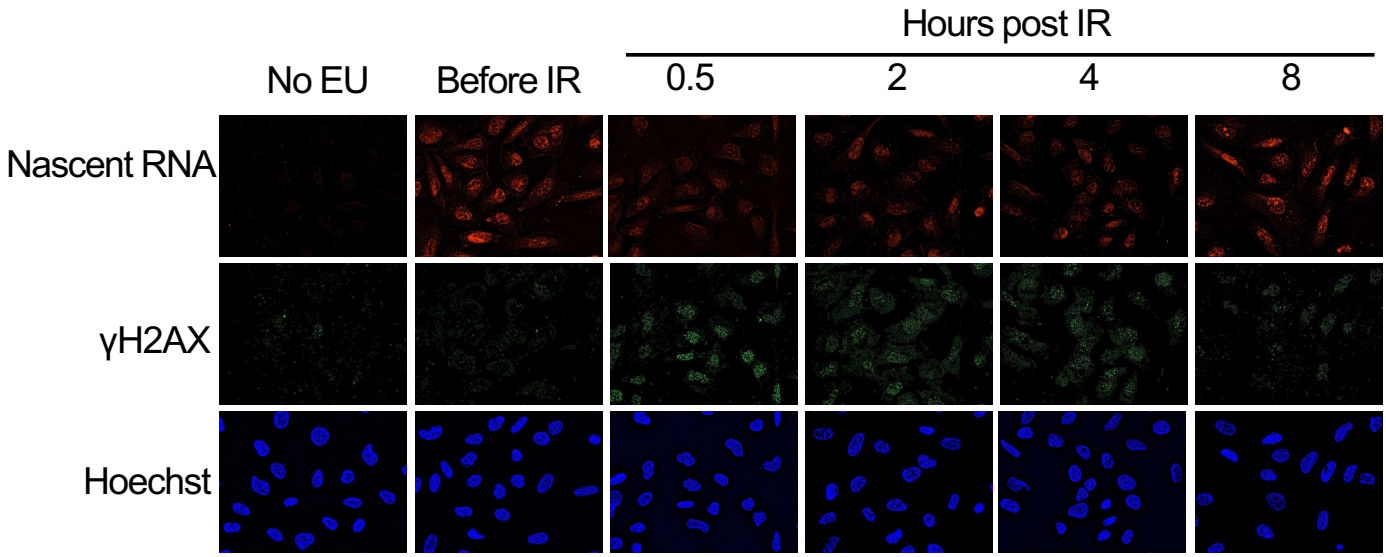
Hours post IR
No EU
Before IR
0.5
2
4
8
Nascent RNA
γH2AX
Hoechst

**Supp Fig. 2**

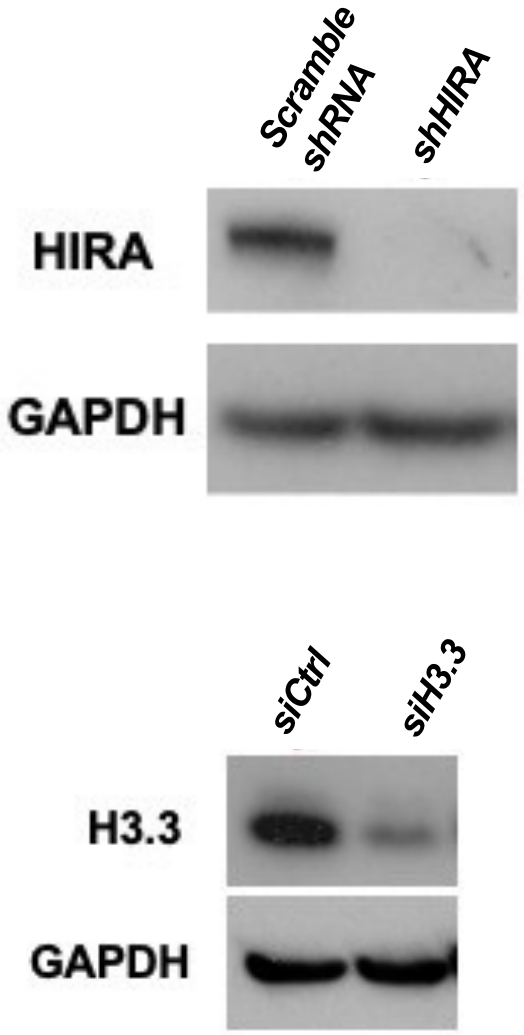

**Supp Fig. 3**

| Dose | No EU | No IR | 15 m | 30 m | 1 h | 2 h | 4 h |
|---|---|---|---|---|---|---|---|
| 2 Gy | 314 | 2690 | 1440 | 1261 | 1282 | 1640 | 2349 |
| 5 Gy | 314 | 2690 | 1379 | 1169 | 1101 | 1345 | 2004 |
| 10 Gy | 314 | 2690 | 1224 | 1094 | 1053 | 1347 | 1803 |

**Supp Fig. 4**

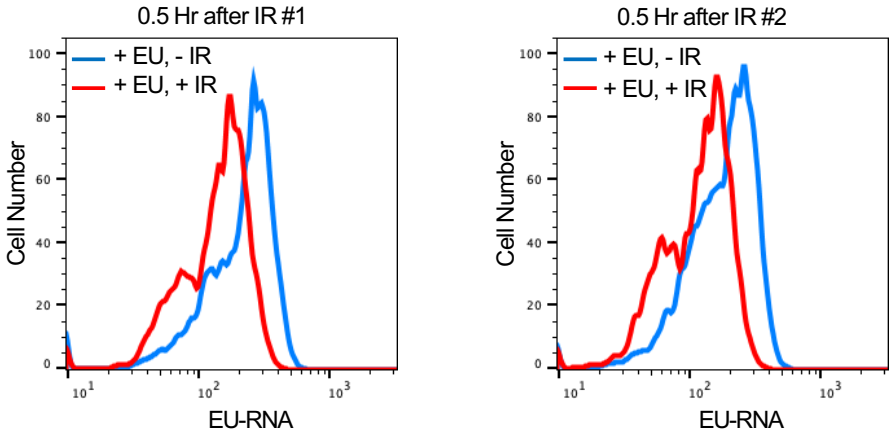
0.5 Hr after IR #1
+ EU, - IR
+ EU, + IR
Cell Number
EU-RNA
0.5 Hr after IR #2
+ EU, - IR
+ EU, + IR
Cell Number
EU-RNA

**Supp Fig. 5**

**A**

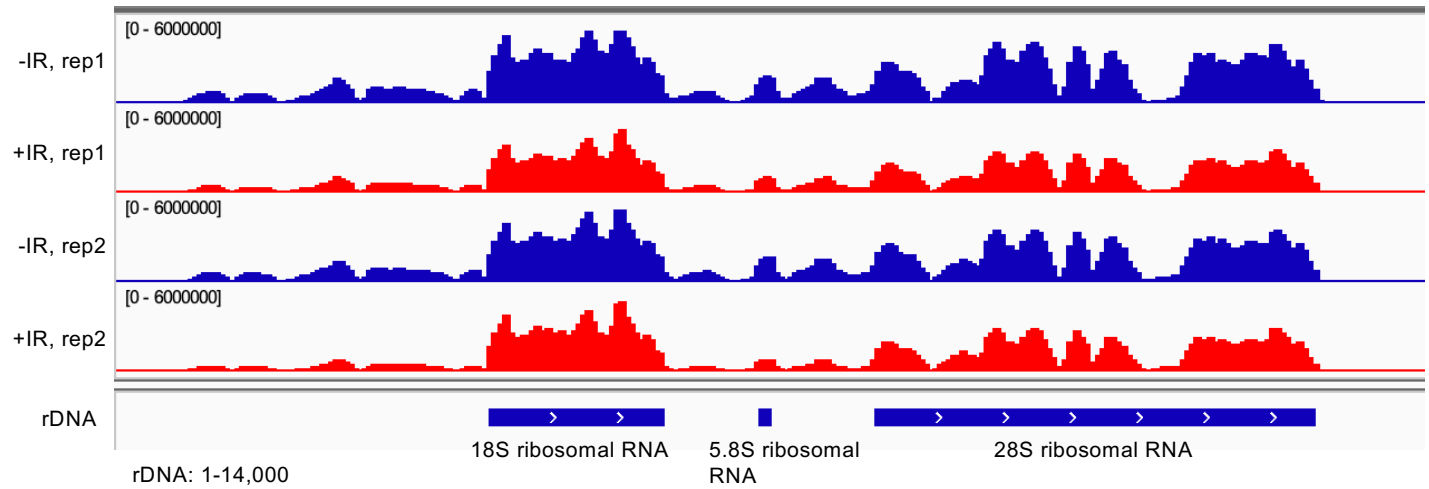
-IR, rep1
[0 - 6000000]
+IR, rep1
[0 - 6000000]
-IR, rep2
[0 - 6000000]
+IR, rep2
[0 - 6000000]
rDNA
18S ribosomal RNA
5.8S ribosomal RNA
28S ribosomal RNA
rDNA: 1-14,000

**B**

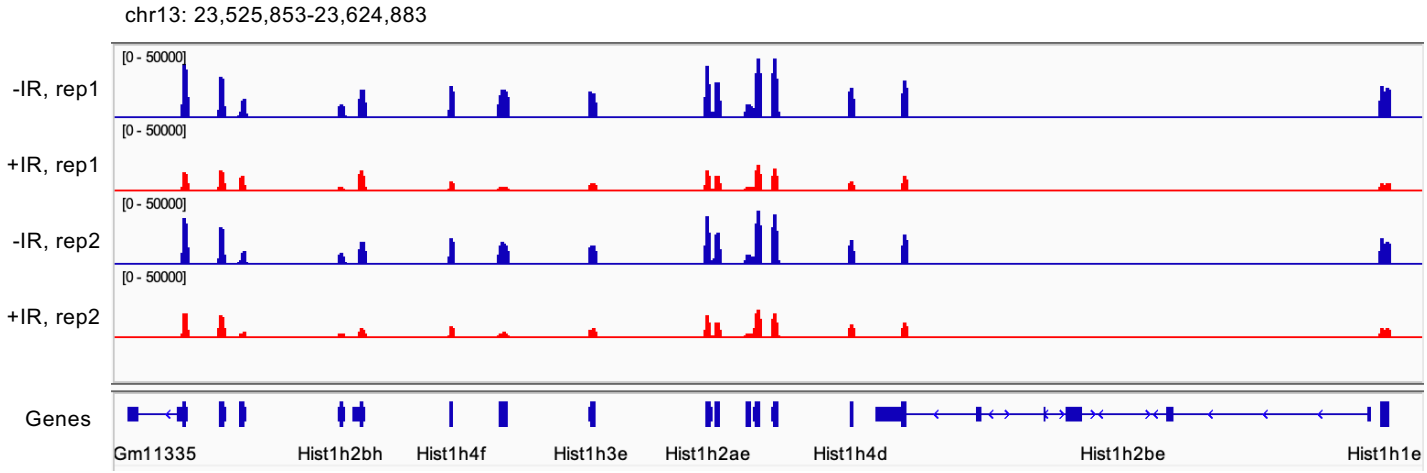
chr13: 23,525,853-23,624,883
-IR, rep1
[0 - 50000]
+IR, rep1
[0 - 50000]
-IR, rep2
[0 - 50000]
+IR, rep2
[0 - 50000]
Genes
Gm11335
Hist1h2bh
Hist1h4f
Hist1h3e
Hist1h2ae
Hist1h4d
Hist1h2be
Hist1h1e

**Supp Fig. 6**

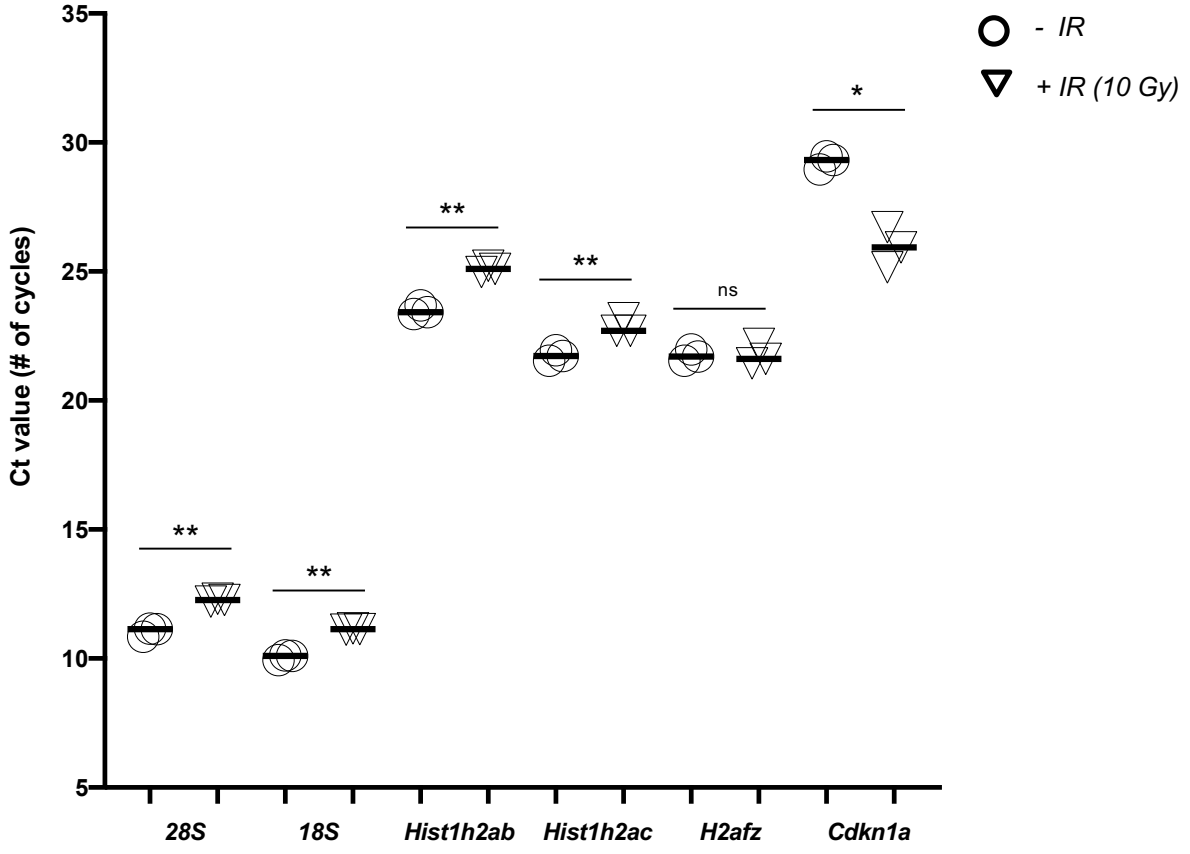
35
30
25
20
15
10
5
Ct value (# of cycles)
**
**
**
**
ns
*
28S
18S
Hist1h2ab
Hist1h2ac
H2afz
Cdkn1a
- IR
+ IR (10 Gy)

**Supp Fig. 7**

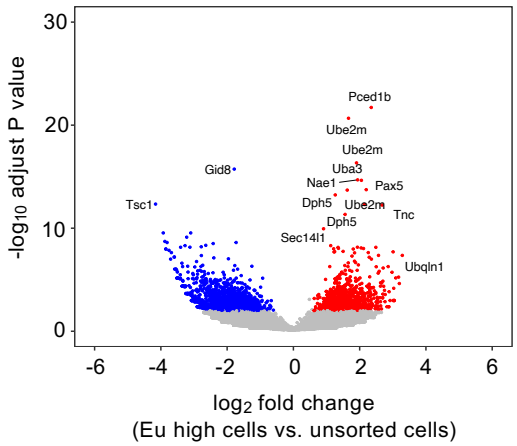
30
20
10
0
-log10 adjust P value
Pced1b
Ube2m
Ube2m
Gid8
Uba3
Nae1
Pax5
Tsc1
Dph5
Ube2m
Tnc
Dph5
Sec14l1
Ubqln1
-6
-4
-2
0
2
4
6
log2 fold change
(Eu high cells vs. unsorted cells)

**Supp Fig. 8**

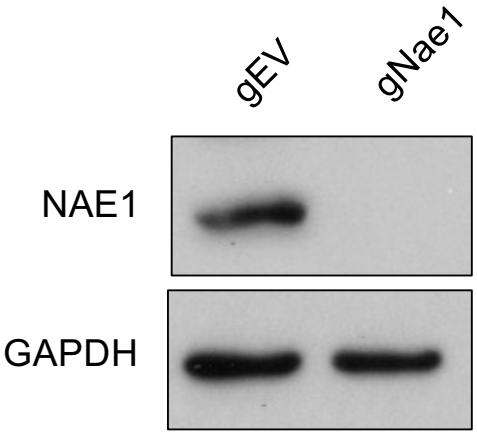

**Supp Fig. 9**

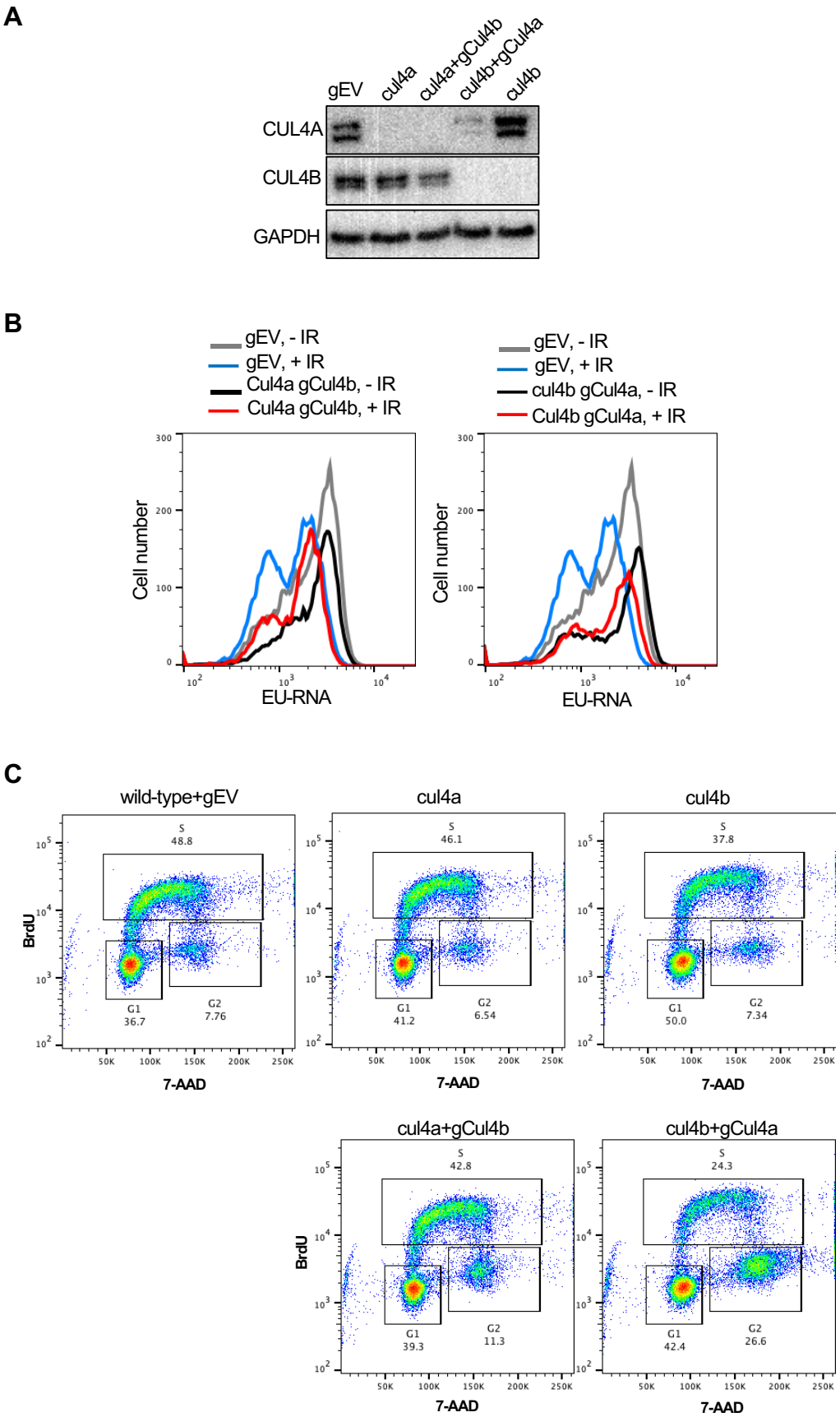
A
gEV
cul4a
cul4a+gCul4b
cul4b+gCul4a
cul4b
CUL4A
CUL4B
GAPDH
B
gEV, - IR
gEV, + IR
Cul4a gCul4b, - IR
Cul4a gCul4b, + IR
gEV, - IR
gEV, + IR
cul4b gCul4a, - IR
Cul4b gCul4a, + IR
Cell number
EU-RNA
C
wild-type+gEV
cul4a
cul4b
cul4a+gCul4b
cul4b+gCul4a
BrdU
7-AAD
S 48.8
G1 36.7
G2 7.76
S 46.1
G1 41.2
G2 6.54
S 37.8
G1 50.0
G2 7.34
S 42.8
G1 39.3
G2 11.3
S 24.3
G1 42.4
G2 26.6

**Supp Fig. 10**

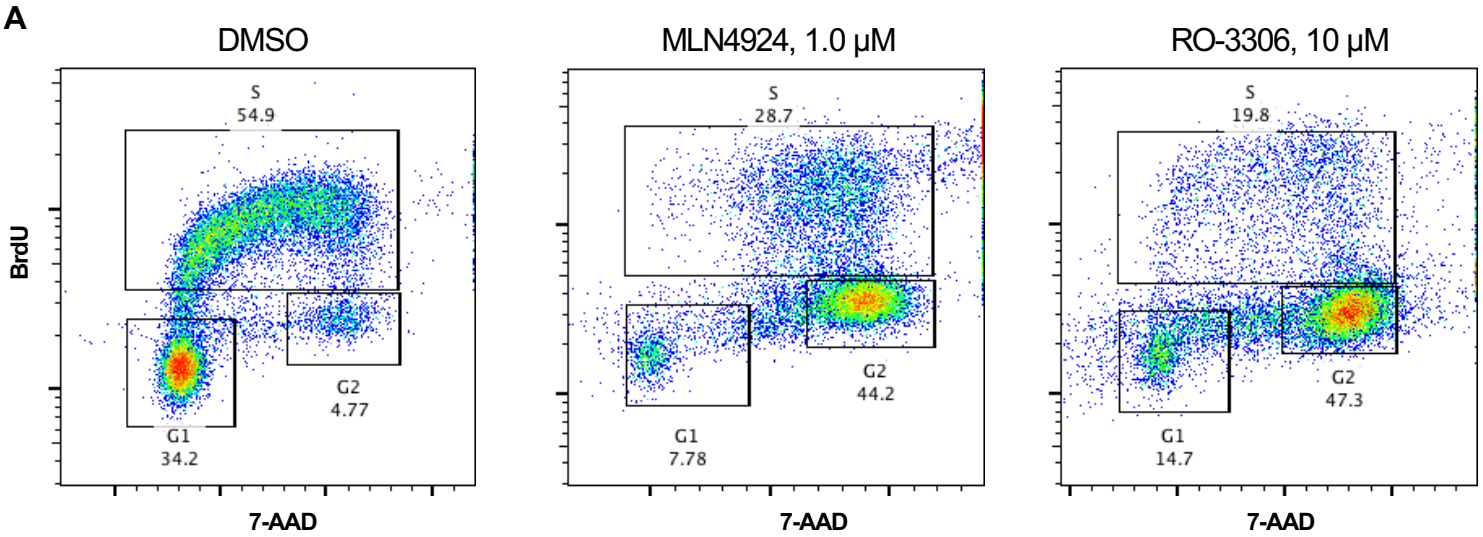
A
DMSO
MLN4924, 1.0 μM
RO-3306, 10 μM
BrdU
7-AAD
S
54.9
G2
4.77
G1
34.2
S
28.7
G2
44.2
G1
7.78
S
19.8
G2
47.3
G1
14.7

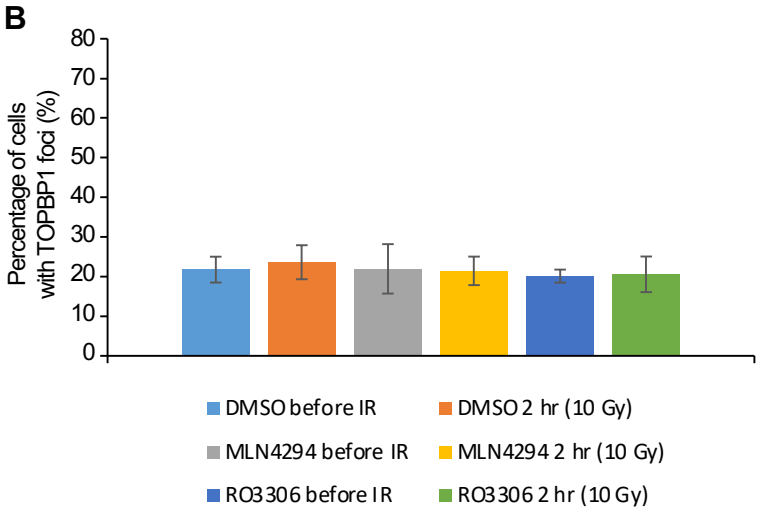
B
Percentage of cells with TOPBP1 foci (%)
80
70
60
50
40
30
20
10
0
DMSO before IR
DMSO 2 hr (10 Gy)
MLN4294 before IR
MLN4294 2 hr (10 Gy)
RO3306 before IR
RO3306 2 hr (10 Gy)